Structural analysis of four cyclic antimicrobial hexapeptides in aqueous solution and in micelles, towards membrane-mimicking nanodiscs

Fredrik Garnås Rylandsholm,[1] Philip Rainsford,[1,3] Monika Krupova,[1,4] Tone Kristoffersen,[1] Tonje Haugen, [1,4] Bjørn Olav Brandsdal,[1,4] John Sigurd Svendsen,[1] Johan Isaksson[1,2]*

[1] *Department of Chemistry, Faculty of Science and Technology, UiT The Arctic University of Norway, N-9037 Tromsø, Norway*

[2] *Department of Pharmacy, Faculty of Health Sciences, UiT The Arctic University of Norway, N-9037 Tromsø, Norway*

[3] *Department of Biomedical Sciences, Faculty of Health and Medical Sciences, University of Copenhagen, Panum Building 18.5. Blegdamsvej 3B, 2200, Copenhagen, Denmark*

[4] *Hylleraas Centre for Quantum Molecular Sciences, Department of Chemistry, UiT The Arctic University of Norway, N-9037 Tromsø, Norway*

Abstract

Cationic, antimicrobial peptides (AMPs) are abundantly present in nature as host-defensive peptides, forming the backbone of the natural defence of many organisms. Their primary interaction with bacterial membranes is thought to be a binding to the outer layer, followed by a disruption of the lipid membrane. Investigating the mode-of-action of AMPs is an ever-growing field, where a plethora of different biophysical experiments are used to investigate this. Here, we explore the experimental limitation in NMR spectroscopy as we migrate towards increasingly realistic but larger membrane model systems with the aim to scout which data we could realistically extract from AMPs interacting with self-aligning nanodiscs.

A set of cyclic hexapeptides were used as model compounds, in water, DMSO, and SDS micelles. The quality of isotropic and anisotropic NMR parameters decreased as the result of faster relaxation due to size and dynamics, as well as the need for water suppression and buffer salts. Chemical shifts, scalar couplings, NOE derived distances, and simulated annealing suggested that the backbone conformation of both peptides remained mostly rigid, forming two

β-turns, while the sidechains remain flexible in all environments. The difference between Lys or Arg did not change the backbone conformation, even though the two peptides have different MIC concentrations, indicating that amino acid composition is more important than conformation for antimicrobial activity. Theoretical structures in an explicit lipid bilayer were simulated showing similar structures.

Pilot experiments on SMA-QA nanodiscs indicated that they are viable as membrane model for investigating the interaction between AMPs and lipid membranes. It was shown that signal can be obtained from bound peptide, but further investigations with isotopically labelled peptides are needed to extract relevant structural data under conditions where the nanodisc is not over-saturated by peptides.

Introduction

Antimicrobial peptides are a part of our innate and non-adoptive immune system, and serve as the first line of defence versus a variety of organisms.[1] In this class, cationic antimicrobial peptides are over-represented and have been found to possess a broad spectrum of activity against bacteria, fungi, protozoa, enveloped viruses, malignant cells and parasites.[2, 3] Antimicrobial peptides make up a group of diverse molecules ranging from approximately 10 to 100 amino acids, having a net positive charge, often along with an amphipathic structure.[4] Despite their similar overall physical properties little sequence homology is observed.[5]

In the light of the emerging antimicrobial resistance crisis, where our existing arsenal of antibiotics is becoming less and less efficient, the importance of potential new classes of antibiotics cannot be emphasised enough. An interesting feature of this class of peptides is that they physically destabilise cellular membranes with a preference for prokaryotic organisms, through a general mechanism (like for example Daptomycin,[6] Nisin,[7-12] and Colistin[13-15]) instead of a well-defined bacterial target like most antibiotics on the market today (for example beta-lactams,[16-20] tetracyclines,[18] quinolines, and amphenicols[21]). Cationic, antimicrobial peptides (AMPs) have proven more resilient to bacterial resistance development,[3] and although this view has been challenged,[22] even if resistance development against AMPs merely comes at a higher fitness cost, they are still an attractive class of compounds for further optimisation into antibiotic leads.

Most of the AMPs reported in the literature are proposed to act directly on the bacterial outer membrane and through the formation of pores, toroidal pores or collapsing carpets, either by reducing the membrane integrity to the point that extensive leakage leads to cell death, or by depolarising the electric gradient necessary to power essential bacterial intracellular processes.[12, 23-27]

There are several examples in the literature where AMPs change conformation and/or physicochemical properties when they come into contact with amphipathic environments like the bacterial cell surface, sometimes mimicked by micelles or liposomes in structural studies.[28-33]

Nuclear magnetic resonance (NMR) spectroscopy is an information-rich and versatile tool that is routinely used to extract structural information from molecules. Chemical shifts hold information about the local chemical environment.[34] $^{3}J_{HH}$-coupling constants are used to investigate the dihedral angle between two protons, and yields much information about the backbone of peptides.[35, 36] Secondary chemical shifts are a good probe for the overall structure of a peptide, being used to describe the secondary structure by comparison between experimentally obtained chemical shifts and random coil reference shifts.[37-45] Nuclear Overhauser effect (NOE) derived distances show correlations through space, allowing for analysis of the 3D structure of molecules.[46]

A technique that has gained more traction in the last few decades is anisotropy, where induced order is forced upon the sample, usually through a liquid crystal (LC) or a strain-induced alignment in a gel (SAG), allow for measurement of a global alignment tensor through residual dipolar coupling (RDC), residual chemical shift anisotropy (RCSA), and residual quadrupolar coupling (RQC).[47-60] Using anisotropic parameters can be used to distinguish enantiomers or diastereomers.[51, 58, 61-63] The anisotropic NMR parameters are dependent on an assembly of theoretical structures to distinguish between.[60]

Theoretical conformations are generally generated in two different ways.[64-67] The first involves an extensive conformational search by *ab initio* computations. The resulting conformers are then geometry optimised, and corresponding structural information that can be used to compare to experimental data is calculated from the finalised structures. The second method involves using experimentally obtained data, such as NOE derived distances or *J*-coupling constants, as constraints in the calculations. Both methods have advantages and disadvantages but are usually

done with different intentions in mind: Simulating data that experimental data can be compared to in case of uncertainty, or creating conformers from the experimental data to get an idea of how the molecule behaves in different environments, or when binding to a ligand.

In this work we aimed to explore which NMR parameters we could extract and how sensitive they are to the conformation in aqueous solution and in multiple model systems mimicking the bacterial surface. We have employed a test set of cyclic AMPs provided by an associated project[68-70] to probe their conformation in water, DMSO, SDS, and nanodiscs.

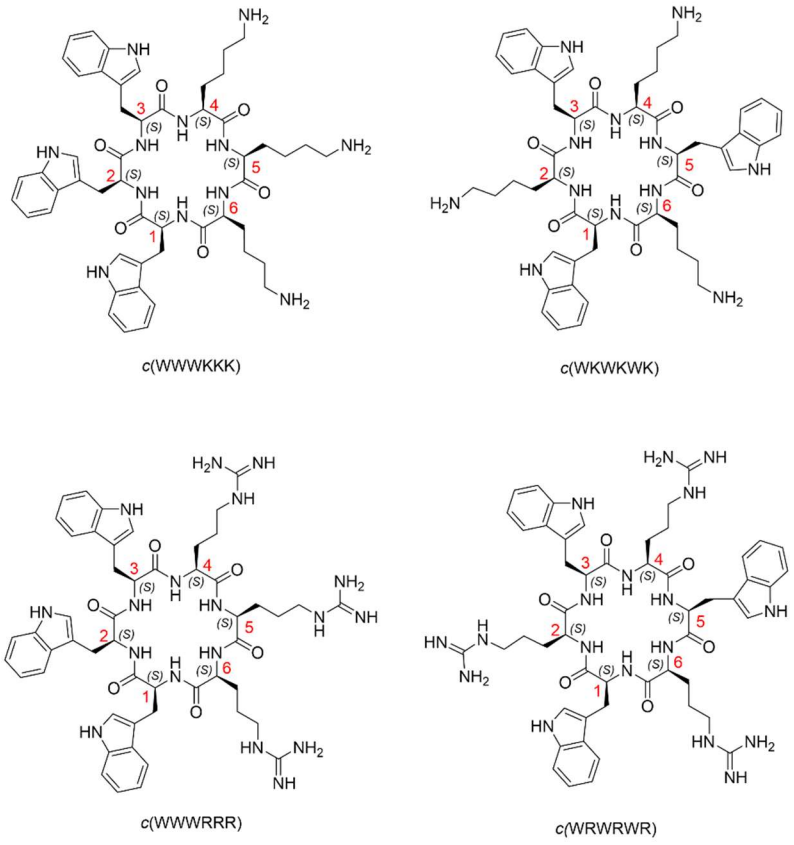

*Figure 1. The chemical structures of peptides **1-4**.*

Results

Conformational analysis in aqueous solution

The baseline conformations of peptides 1-4 in aqueous solvent as well as dmso has been briefly described in a previous work from our lab.[70] The main characteristics of the peptides were that

they displayed relatively small conformational backbone variations as a function of their amino acids sequence. The measured NMR parameters, reproduced in Tables S1-S12 in the Supporting materials.

The chemical shifts in aqueous buffer were compared to the chemical shifts in SDS micelles. Changes in the order of half a ppm were observed for multiple residues, and the general trend was that lysine containing peptides became more deshielded, while arginine containing peptides became more shielded in SDS compared to aqueous buffer (Table 1). Backbone amide changes like these are commonly dominated by the relation to the backbone carbonyl, which can be both shielding and deshielding, plus any changes in contributions from hydrogen bonds, where hydrogen bonds have a deshielding effect.

*Table 1. Chemical shifts of the amides of peptides **1-4** in water, DMSO and in SDS micelles.*

	c(WWWKKK)						c(WWWRRR)					
	Water		DMSO		SDS		Water		DMSO		SDS	
	^{1}H (PPM)	^{15}N (PPM)	^{1}H	^{15}N	^{1}H	^{15}N	^{1}H	^{15}N	^{1}H	^{15}N	^{1}H	^{15}N
1	7.85	118.0	8.07	116.2	8.12	119.1	7.88	118.0	8.04	116.6	8.03	118.8
2	7.33	119.0	7.94	117.0	7.91	116.7	7.42	119.0	7.96	117.2	7.40	127.06
3	7.55	121.2	8.20	118.8	7.91	116.7	7.64	121.2	8.22	118.0	7.17	-
4	7.84	120.8	8.21	116.7	7.81	120.2	7.94	120.2	8.32	116.90	7.71	120.81
5	8.03	119.5	8.00	115.2	7.92	116.7	8.15	119.0	8.18	116.0	7.93	116.93
6	7.77	119.4	8.03	116.6	7.22	117.7	7.87	119.5	8.11	116.5	7.29	117.44
	c(WKWKWK)						c(WRWRWR)					
	Water		DMSO		SDS		Water		DMSO		SDS	
1	7.99	119.3	8.15	117.1	-	-	8.07	119.4	8.15	116.8	7.31	-
2	7.62	120.2	8.03	116.7	-	-	7.65	120.0	8.11	116.9	7.19	-

To visualise the significance of the amplitude of the chemical shift changes, TALOS+(N) was used to predict the phi/psi angles as well as the secondary structures implied by the changes in observed chemical shifts (Figure 1). It should be noted that TALOS is parametrised on large well folded proteins and may have poor accuracy when applied to small cyclic peptides. Especially if the cyclisation pushes the peptide into normally less populated states. Nevertheless, it gives an indication as to what amplitude of chemical shift changes are

associated with changes in secondary structure and the phi/psi dihedral angles. TALOS+(N) predicts significant changes in secondary structure between water and SDS for the arginine containing peptides (Figure 2). These predictions were however in poor agreement with the three state phi/psi distribution predictions in TALOS+(N) using the same input data (Figure S 7 and Figure S 8), which warranted a more detailed investigation into their conformations in different environments by other NMR observables.

Figure 2. Neural network secondary structure prediction in TALOS+(N) as fractions of alpha helix (blue), beta sheets (orange), and loop (grey) secondary structure types, proposing a higher degree of folded helix-like conformations in SDS compared to water for the arginine containing peptides.

The $^{3}J_{HNHA}$ scalar couplings provide information about the phi dihedral angle. In peptides and proteins, the most commonly populated angles are approximately -60 degrees for alpha helices and 310-helices corresponding to a *J*-coupling of ~4 Hz, and approximately -120-(-140) degrees for beta sheets corresponding to ~9 Hz.[71] The measured couplings, presented in Table 2, did not suggest as much alpha helix (folded) character as the chemical shifts alone did in water for

the three-state distribution model in TALOS+(N) (Figure 3). The peptides instead predominantly displayed couplings somewhere in between the average values of the common defined secondary structures, which would fit better with the direct secondary structure prediction in TALOS+(N) (Figure 2). The Ramachandran plot of the phi/psi low energy space does show that there is overlap between the alpha helix- and the beta sheet regions with regards to phi angle alone, allowing the full range from –140 to -60, so there is no contradiction between the measured intermediate size of the couplings and either alpha helices or beta sheets, including the more unusual left-handed helices. It is also plausible that the small cyclic peptides maintain some flexibility in the cyclised form and display a time averaged coupling. There was a weak trend that peptides containing arginine displayed a slightly stronger preference for folded conformations (alpha helix like) than the lysine containing peptides did, as reflected by their average couplings being lower, and thus closer to 4 than to 9. The trend was also that several residues of the arginine containing peptides experienced 1-2 Hz changes in coupling constants when going from water to DMSO. This could indicate that a larger fraction of the time is spent in more extended beta sheet like conformations with phi angles in the -120 degrees range. The resolution was insufficient in SDS to allow of any line shape simulations to reliably extract the J_{HNHA} coupling constants without making excessive assumptions about the line width of the exchangeable amide protons.

Table 2. $^{3}J_{HNHA}$ coupling constants for peptides 1-4 in water and DMSO.

Resid	Water				DMSO			
	c(WWWKKK)	c(WKWKWK)	c(WWWRRR)	c(WRWRWR)	c(WWWKKK)	c(WKWKWK)	c(WWWRRR)	c(WRWRWR)
1	7.0#	7.1	7.9#	6.2	6.5	7.1	8.3	7.6
2	6.9#	6.2*	5.4*	5.8	7.1	6.9	7.4	6.7
3	6.2*	7.1	5.1*	6.2	8.2#	7.1	7.1	7.6
4	5.7#	6.2*	6.2	5.8	6.8#	6.9	7.2	6.7
5	7.5	7.1	7.6	6.2	7.6	7.1	7.9	7.6
6	6.2	6.2*	6.2#	5.8	5.9	6.9	7.3	6.7

lineshape fitted from a high resolution and zero filled ^{15}N-HSQC F2 slice

* lineshape fitted from an unresolved doublet

NOE build-up between two protons is inversely proportional to the distance between them to the power of six (r^{-6}). For backbone structure, the most informative distances are those between HN-HN(n-1) which are ~2.8 Å in a helix and ~4.3 Å in a sheet, and HN-HA(n-1), which are ~3.5 Å in a helix and ~2.2 Å in a sheet. We would thus expect very strong NOE correlations between HN and HA(n-1) in beta sheet like structures and between HN and HN(n-1) in alpha helix like structures. The measured NOE buildups, translated into distances using the two-proton approximation with aromatic tryptophan crosspeaks as reference, are reported in Table 3. The NOE distances indicated no major changes in conformation between water and DMSO for either peptide. If anything, a somewhat strengthened extended conformation in DMSO. However, in SDS there is a significant increase in HN-HA(n-1) distances for the arginine containing peptides, suggesting a change in secondary structure towards a more folded form than in water, which is again in agreement with the direct secondary structure prediction from TALOS+(N) (Figure 2). Note that distances for residues 3 and 4 for this peptide are ambiguous due to spectral overlap.

*Table 3. HN-Hα(n-1) distances of peptides 1 and 4 in different environments from NOE buildup experiments, given in Å. *overlapping peaks.*

c(WWWKKK)						
	W1	W2	W3	K4	K5	K6
Water	2.83	3.01	3.28	**2.45**	3.03	2.83
DMSO	2.52	2.61	2.17*	2.17*	2.85	2.32
SDS	2.58	-	3.11	**4.65**	3.15	3.25
c(WWWRRR)						
	W1	W2	W3	R4	R5	R6
Water	2.85	**2.95**	3.39	**3.01**	**3.48**	**3.28**
DMSO	3.09	2.83	2.93	3.27	3.30	3.13
SDS	3.50	**4.17**	-	**4.08**	**4.00**	**4.50**

Conformational analysis by structure calculations

Structure calculations were performed using X-PLOR, introducing different NMR-derived constraints in the different environments; water, DMSO and SDS. Initially, the structures were based entirely on NOE constraints. Subsequently, scalar coupling constraints were introduced, and finally test calculations adding TALOS derived phi/psi dihedral constraints were performed

to evaluate their accuracy. The generated structures are presented in Figure 3, with the averaged structures found in the Supporting Information (Figure S 9).

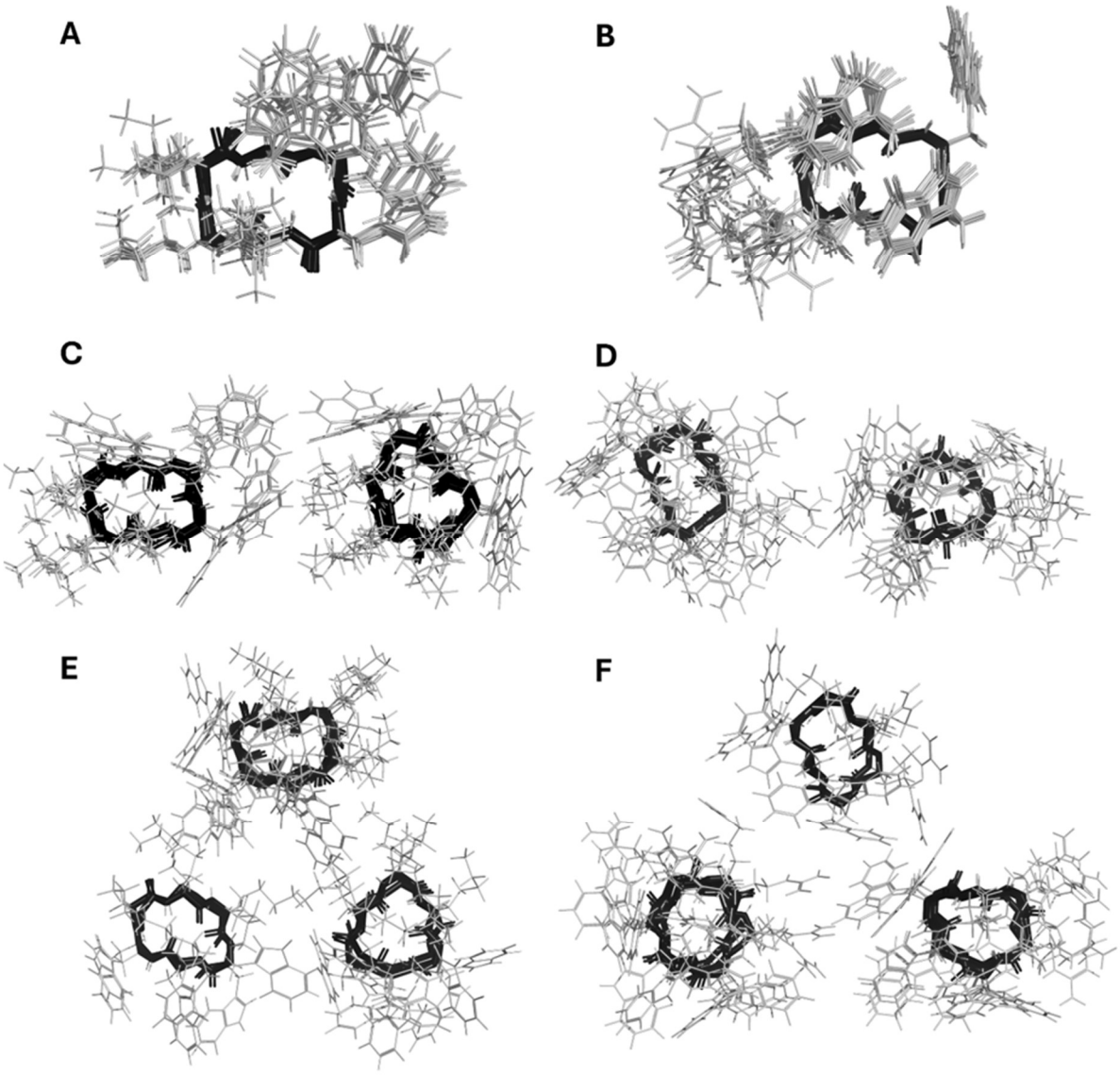

Figure 3. Superimposed representations of the ten lowest energy conformations based on NOE constraints of (A) c(WWWKKK) in water; (C) c(WWWKKK) in DMSO; (E) c(WWWKKK) in SDS ; (B) c(WWWRRR) in water; (D) c(WWWRRR) in DMSO; c(WWWRRR) in SDS.

Both peptides primarily adopt conformations consisting of two β-turns with the i+1 and i+2 residues being the same amino acid. *I.e.*, the turns occur between two Trps and two Lys/Arg. This is consistent with structures of similar cyclic hexapeptides reported in the literature.[28, 72]

In DMSO and SDS additional conformations are more prevalent. While the coupling constants and NOEs suggests that changes in populations may very well occur when moving from water to SDS, we are at the same time getting significantly fewer experimental constraints in the latter, and therefore the additional conformations can also be the effect of less constrained simulations. In either case, the constraints could be satisfied by multiple conformations. In some cases, the additional conformations are still two β-turns with the turns occurring between Trp and Lys/Arg residues resulting in the clustered residues running parallel to one another

Table 4. Pairwise root mean square deviation (RMSD) calculated for the top-10 structures in different solvents to demonstrate the variance in the structure generation. NOE structures are those presented in Figure 3. NOE – NOE constraints only. NOE + CC – NOEs and coupling constants as constraints. NOE + CC + Diheds – NOEs, coupling constants and TALOS predicted dihedral angles as constraints.

	Water RMSD (Å)			DMSO RMSD (Å)			SDS RMSD (Å)
	NOE	NOE + CC	NOE + CC + Diheds	NOE	NOE + CC	NOE + CC + Diheds	NOE
WWWKKK	0.18 +/- 0.06	0.17 +/- 0.06	0.05 +/- 0.02	0.98 +/- 0.29	0.75 +/- 0.33	1.49 +/- 0.61	1.31 +/- 0.41
WWWRRR	0.11 +/- 0.00	0.03 +/- 0.00	0.02 +/- 0.00	0.38 +/- 0.00	0.58 +/- 0.00	0.65 +/- 0.00	0.18 +/- 0.00

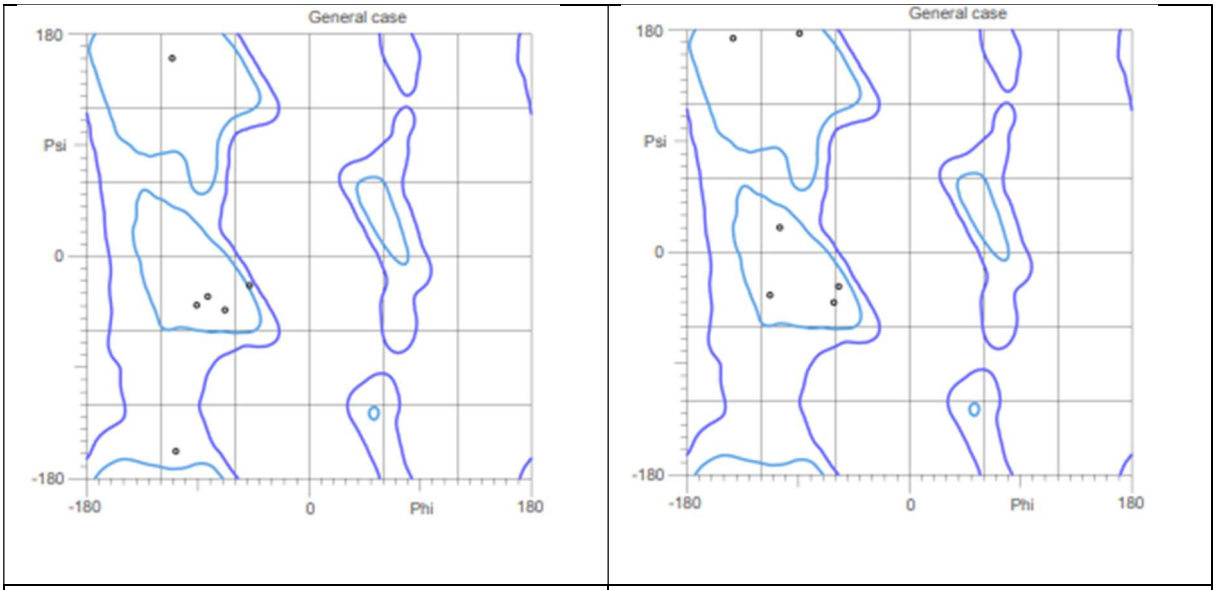

(a) (b)

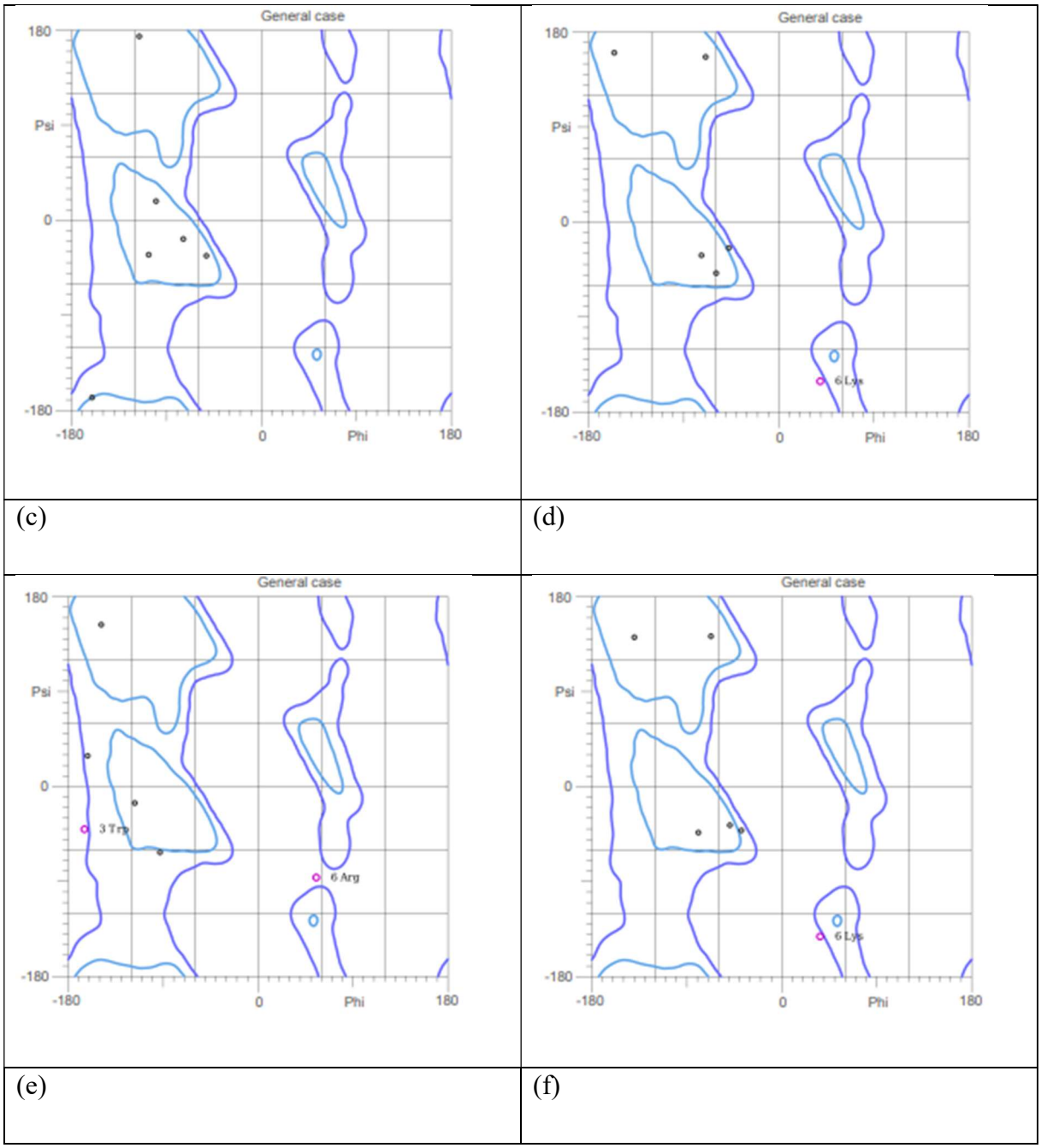

Figure 4. Ramachandran plots of (a) cWWWRRR in water, (b) cWWWKKK in water, (c) cWWWRRR in DMSO, (d) cWWWKKK in DMSO, (e) cWWWRRR in SDS and (f) cWWWKKK in SDS.

The introduction of the experimentally derived coupling constants as structural constraints alongside the NOEs during structure generation introduces a modest increase in the potential energy of the structures. However, when the TALOS predicted bond angles are subsequently added as a constraint, the potential energies are significantly higher. This effect is much more exaggerated in the DMSO-based structures, which is to be expected since the predictions are based on NMR data of proteins in aqueous conditions. It was therefore concluded that the three-

state predictions of phi/psi angles in TALOS+(N) were not consistent with the other experimental observations and did not contribute positively to structure calculations.

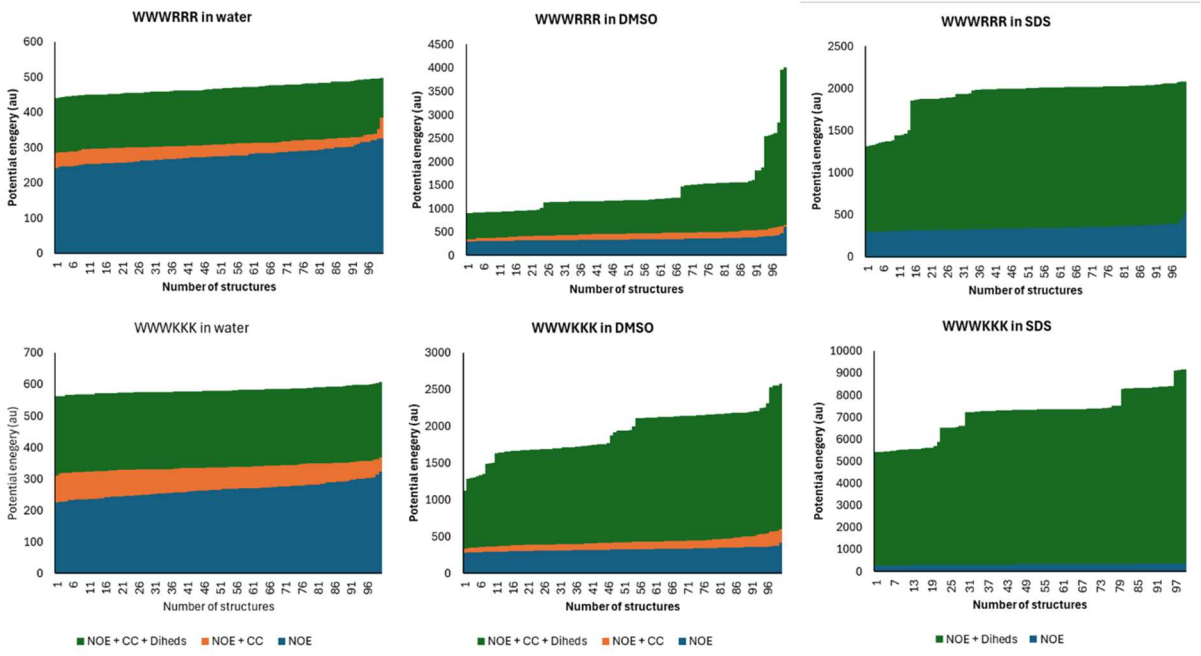

Figure 5. Potential energies of the 100 generated structures by the simulated annealing protocol in descending order using different constraints. NOE – NOE constraints only. NOE + CC – NOEs and coupling constants as constraints. NOE + CC + Diheds – NOEs, coupling constants and TALOS predicted dihedral angles as constraints.

Molecular dynamics (MD) simulations in POPE/POPG membranes

Theoretical MD trajectories of c(WWWRRR) and c(WWWKKK) were simulated in POPE/POPG membranes dissolved in a periodic box with explicit water, sodium and chloride ions to provide some insight into which conformations would be expected as we move towards increasingly realistic membrane models. The simulations revealed that the cyclic hexapeptides existed in an equilibrium between bound and free form, within the 260 ns simulation time of the trajectory, but the bound forms did not reveal any new conformational preferences. Representative structures of the two peptides inside the lipid bilayer are shown in Figure 6. Both peptides adopt a conformation with two beta turns, where the turn is between W1 and W2 for c(WWWKKK) and between W3 and R4 for c(WWWRRR). The general structure agreed with the NMR-constrained structures in water, DMSO and SDS, that all produced double beta turn structures with the turns in different positions. It was therefore concluded that the surrounding media does not significantly affect the energy minimized conformations of these

cyclic hexapeptides but is more likely to affect solubility derived properties like self-aggregation and the populations and/or dynamics between the low energy conformations. The conformations remained stable throughout the simulation, no transitions between conformations with the turns in different positions were observed. It is therefore possible that beta turns in different positions give rise to the two conformations in slow exchange observed in NMR for c(WWWRRR) (see Figure 6).

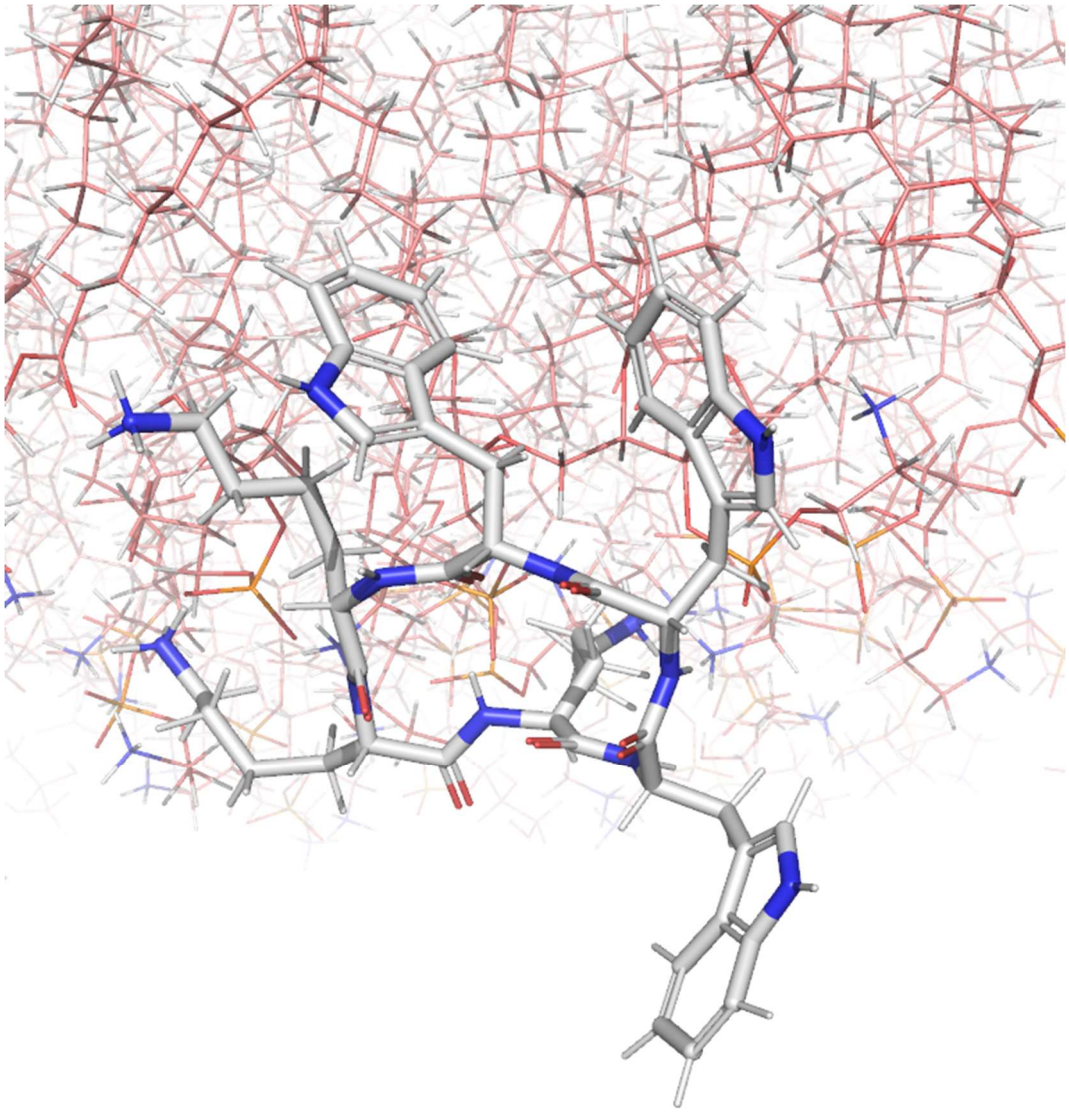

(a)

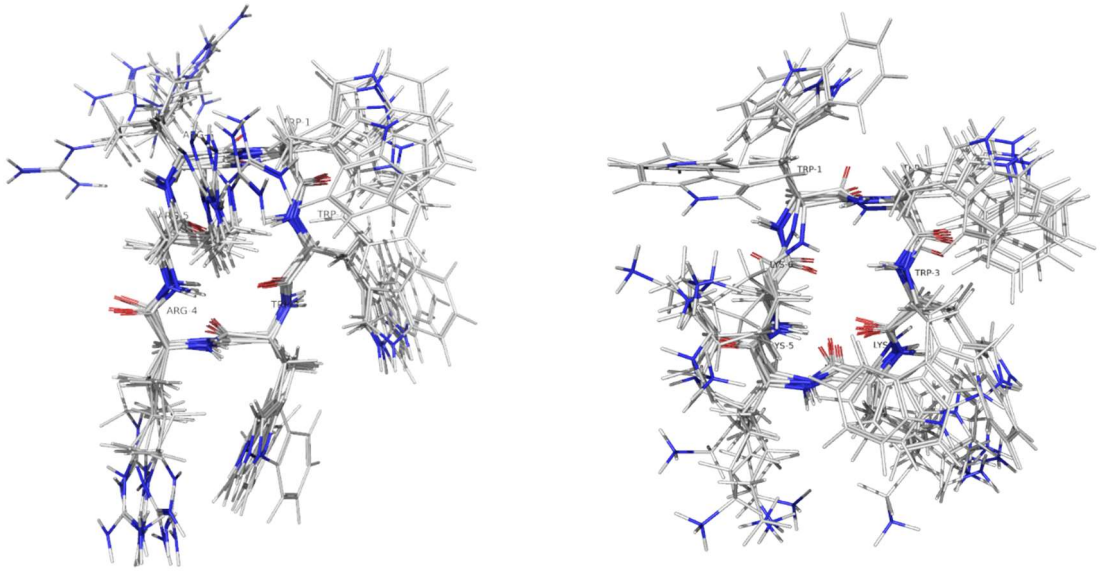

(b) (c)

Figure 6. (a) A representative snapshot of the interaction between c(WWWKKK) and the POPE/POPG bilayer followed by periodically sampled snapshots of the second half of the MD trajectories of (b) c(WWWRRR) and (c) c(WWWKKK).

Slow conformational exchange of c(WWWRRR)

The spectra of peptide c(WWWRRR) displayed one extra set of resonances for several protons and carbons of the peptide with weaker intensity (see Figure 7). Potential epimerisation during the peptide synthesis was ruled out because there were no additional peaks in analytical HPLC, and there was only one extra set, not multiple as you would expect from a random process affecting 6 amino acids. Mass Spectrometry further excluded chemical modification of the peptide. Also, self-aggregation was considered highly unlikely due to it being present in all studied solvents. The extra peaks intensities are approximately in a 1:2 ratio to the main peaks.

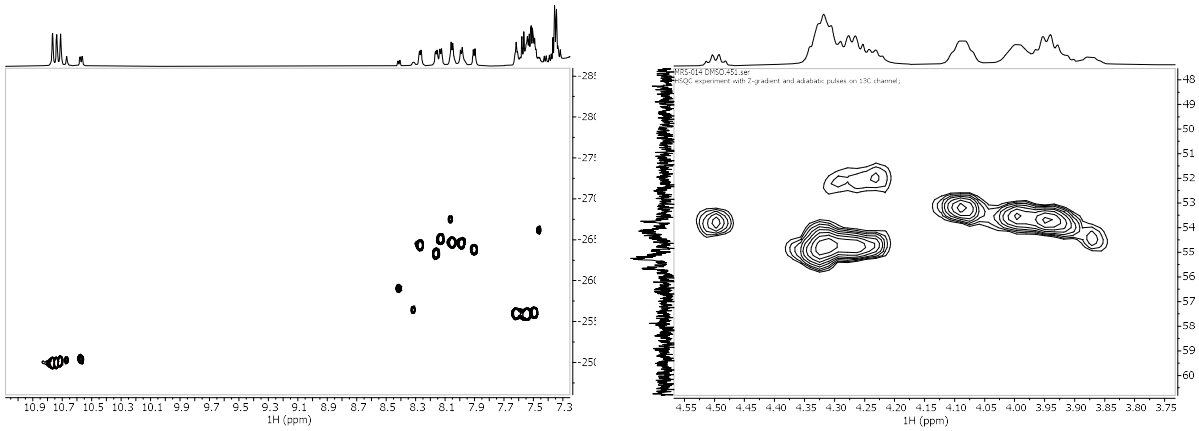

(a) (b)

Figure 7. The ^{15}N-HSQC (a) and the HSQC (b) spectra of the alpha region of c(WWWRRR) in DMSO displaying an extra set of resonances for the backbone NH and CA.

When the temperature was increased from 25°C up to 65°C, several in-phase peaks with the same sign and the diagonal started to appear in ROESY spectra, indicating the presence of very slow exchange between two conformers separated by a high energy barrier (Figure 8).

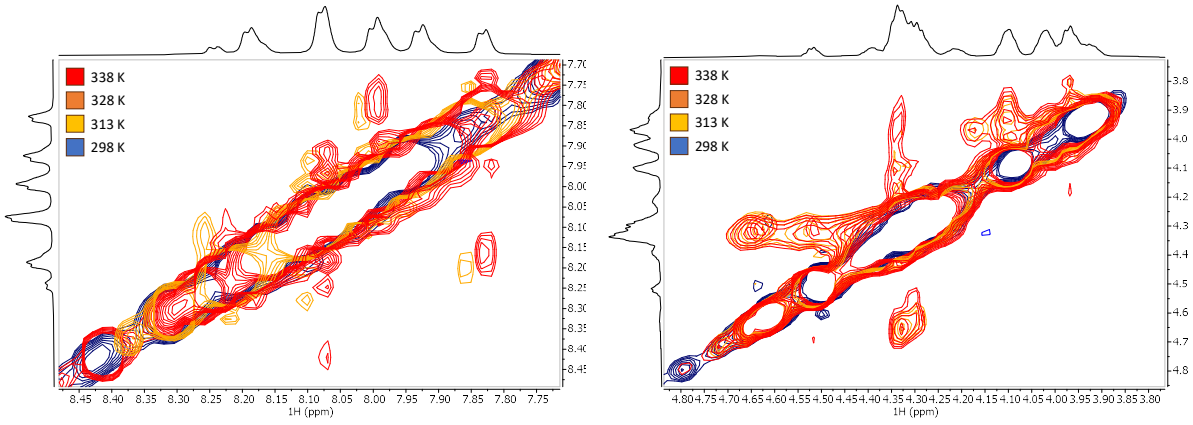

(a) (b)

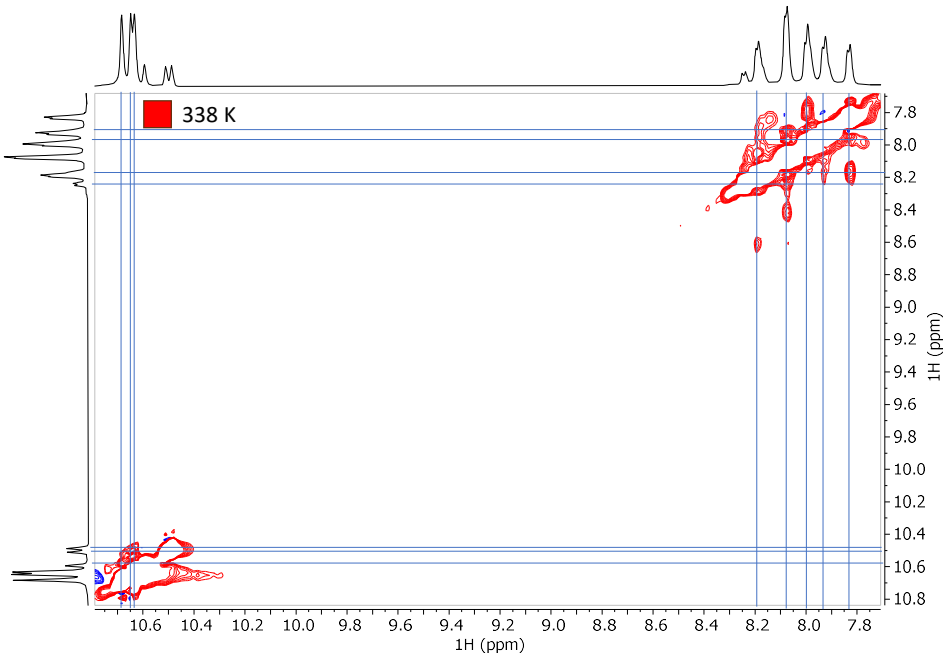

(c)

Figure 8. Expansions of ROESY spectra of c(WWWRRR) in DMSO with 300 ms mixing time at increasing temperatures, showing the HN region (a) and HA region (b), corresponding to the HSQCs in Figure 4. There are multiple crosspeaks in phase with the diagonal that build up with increasing temperature, showing that the peptide is in slow conformational exchange (c) The highest temperature is highlighted to show that crosspeaks connect the major (vertical lines) and minor (horizontal lines) conformations. The projections are given for the ROESY at 338 K, represented in red.

The exchange is present in all studied solvents, in roughly the same populations. The temperature dependent buildup was only studied in DMSO, but there was no apparent lowering in energy barrier between the conformations in the different solvents as neither sample displayed any easily detectable exchange at room temperature between the subspecies. In SDS, especially the Tryptophan sidechains produce very broad peaks, as well as displaying multiple sets of chemical shifts.

SMA-QA nanodiscs

The polymer based SMA-QA nanodiscs have recently attracted attention for displaying self-aligning properties in strong magnetic fields under certain conditions.[73-76] The SMA-QA based nanodiscs were therefore suggested as a more realistic membrane model systems to extract conformational information from, compared to micelles. While traditional micelle model

systems provide excellent spectral quality, there is always the troubling fact that tensides are themselves very different entities compared to phospholipids, and they also behave very differently from phopholipids, self-assembling into small lipid droplets with a high curvature while the phospholipids prefer to form flatter bilayered structures.[77-80] In addition, there is also the uncertainty whether these droplets maintain any of that droplet structure after interacting with moderately sized AMPs, or if they partially or completely disassemble in contact with the AMP and rather solvate the AMP with dispersed lipids interacting in favourable positions across the AMP. It would therefore be highly attractive to access any structural information from any phospholipid-based model system that is stabilised by a scaffold to give resilience against complete disruption by small membrane active compounds.

There are examples in the literature of membrane protein structures being studied in lipid nanodiscs aligned using virus filaments.[81] In the case of the AMPs studied herein however, there are direct interactions between virus filaments and the AMPs, making this approach difficult. The boundary conditions for using SMA-QA nanodiscs in combination with our set of AMPs was therefore explored to probe if conformational studies using isotope labelled peptides could be economically- and practically feasible. In addition to the challenges with concentration, solubility and nanodisc production, the system we were exploring was not a well-defined solubilised protein produced and isolated in 1 to 1 ratio with the nanodisc, but rather an unspecific interaction being gradually added to an already assembled disc.

The original paper describing the assembly and purification of the SMA-QA nanodiscs describe one of the strengths of the nanodiscs to be their very exact size-tuneability.[74] By mixing SMA-QA:lipid at ratios of 1.5:1, 1:1, or 0.25:1 nanodiscs can be assembled with a diameter of 10, 20, or 30 nm, respectively. The size control was first reproduced by mixing the same ratios of SMA-QA polymer and DMPC or DMPC with 5% DMPG. The nanodiscs separated in size exclusion chromatography (SEC) as a distribution of sizes around the target size. Nanodiscs of ~30 nm had a retention time of approximately 50 minutes, ~20 nm and ~10 nm discs had retention times of approximately 70 minutes, and SMA-QA of approximately 115 minutes. The nanodiscs and polymer were detected by UV absorbance at wavelengths 254 and 280 nm, and the polymer was detected by a distinct dip in conductivity (See Figure S 4-Figure S 6 in supporting information). When assembling the nanodiscs, several batches were made in parallel. Large unilamellar vesicles were prepared as 1 mL 20 mM samples in Eppendorf tubes, and they were incubated with SMA-QA from a stock solution. Normally, 2-4 samples were prepared simultaneously, and purified the next day. It was noticed that even when the parallel batches

were prepared identically, there were small changes in the retention times and line widths of the elution spectra, and dynamic light scattering spectra showed that the purified discs could range widely in structure, for example from 15 to 30 nm from the intended 20 nm. Therefore, it was concluded that the SMA-QA:lipid ratios to yield specific sizes are guidelines and that every batch needs to be thoroughly characterised.

Ravula *et al*. showed how the alignment of SMA-QA nanodiscs are dependent on lipid concentration.[76] Therefore, the sample collection area was set to approximately 60% of the centre part of the SEC peak, attempting to exclude the tails where the size deviation is the largest. The collected sample was then concentrated to about half the starting volume and the lipid concentration was determined by ^{31}P NMR. The amount of lipids per disc was estimated from the diameter found by DLS at 30°C, the reference area of the DMPC lipid head group,[82-84] and the width of the SMA polymer.[85] To the best of our knowledge, the width of the SMA-QA polymer has not been reported, hence the width of the SMA polymer was used in the calculations.

SMA-QA nanodiscs have been reported to self-align at higher temperatures,[76] and it could be confirmed that a deuterium splitting was indeed observable above 305 K, reaching a maximum around 310 K (Figure 9). This conveniently coincides with the body temperature, which could be useful for the studies of interactions relevant for an *in vivo* environment. The size of the splitting is also dependent on the size of the nanodisc.

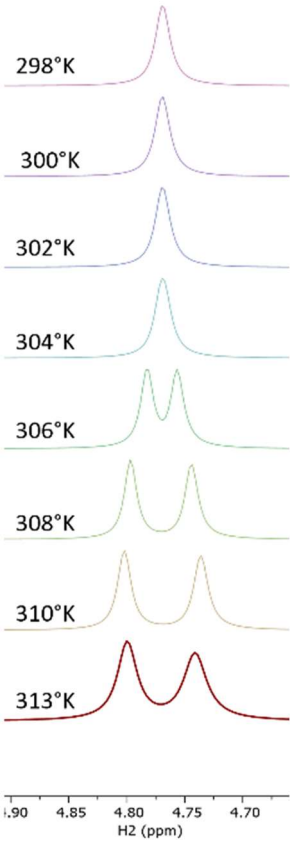

Figure 9. Increase of deuterium signal splitting in a 5 mm NMR tube with increased temperature. The concentration is 6.88 mM lipid in 30.57±12.72 nm SMA-QA DMPC nanodiscs.

The SMA-QA self-alignment also has a concentration and size dependence, and the deuterium doublet quickly collapses when dropping below 115 mM lipid concentration for the shown ~20 nm diameter nanodisc preparation (Figure 10). It was therefore important to ensure that any titration assay did not cause effective dilution of the nanodisc concentration, which can be achieved by adding nanodiscs to the peptide stock, or to assemble the SMA-QA nanodiscs with the AMPs together with the lipids already at the initial nanodisc assembly. Neither of these methods would be unproblematic for membrane active compounds like AMPs but would appear necessary to study interactions with SMA-QA nanodiscs.

It was also observed that the diameter of the sample tube affected the degree of alignment (Figure 10). The splitting collapses at higher concentrations in a 3 mm NMR tube compared to a 5 mm NMR tube, suggesting that the phase of the nanodisc alignment is directly affected by the physical boundaries imposed by the glass walls.

A titration was performed, gradually adding AMPs to a solution of SMA-QA nanodiscs, recording the ^{1}H NMR spectra (Figure 11). Below a 100:1 ratio of AMP per disc, there is virtually no detectable signal arising from the peptides. We interpret this as that the lipid system is being saturated between 100 and 500 AMP:disc ratio (between 20 and 4 lipids per peptide molecule), and at that point the relatively sharp signals from the unbound peptides are detected. It was also concluded that we have an unknown rate of exchange between the bound and the free forms in this system, leading to some but not extensive line broadening of the detectable signals at the extremely high peptide:lipid ratios. The efficiency of signal attenuation all the way up to peptide:lipid ratios in the 100-500 range does however suggest either a very significant k_{ex} rate for efficient time sharing of the high correlation time of the nanodisc complex, or an extremely high binding capacity of the nanodisc constructs themselves, likely through self-aggregation mechanisms on the lipid surface. In addition, the chemical shift and the line width of the bound state is unknown, further complicating any estimates. We do not expect direct interactions between the cationic peptides and the cationic polymer to contribute to the apparent K_D of the complex.

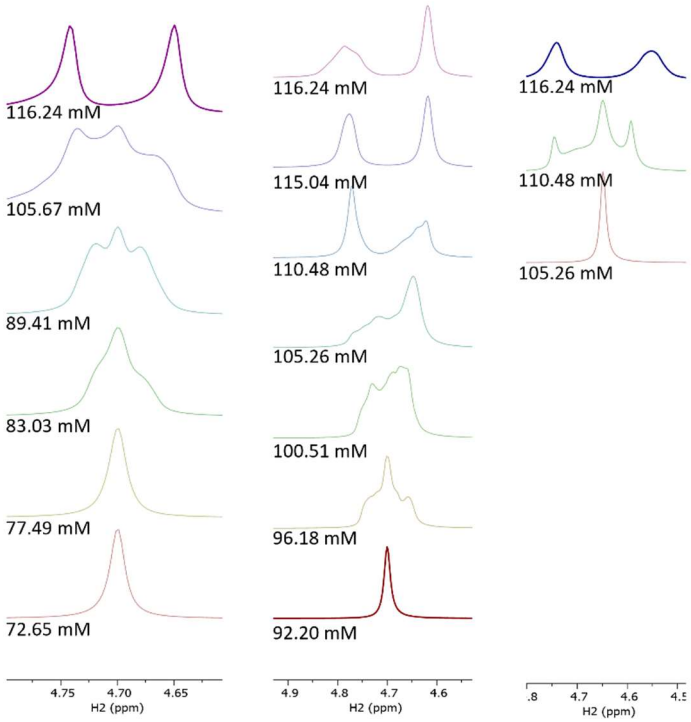

Figure 10. Loss of deuterium signal splitting by dilution in different conditions. (left) Dilution in a 5 mm NMR tube; (middle) dilution in a 3 mm NMR tube; (right) dilution by adding the cyclic tetrapeptide c(WKWKWK) in a 3 mm NMR tube. All NMR spectra were collected at 313 K, the concentrations are lipid concentration, and the size of the SMA-QA DMPC nanodiscs are 20.79±11.14 nm. The dilution in both 3 mm tubes were done by the same volumes, to compare the loss of signal splitting with and without peptide. The dilutions were done with a 90/10 H_2O/D_2O mixture.

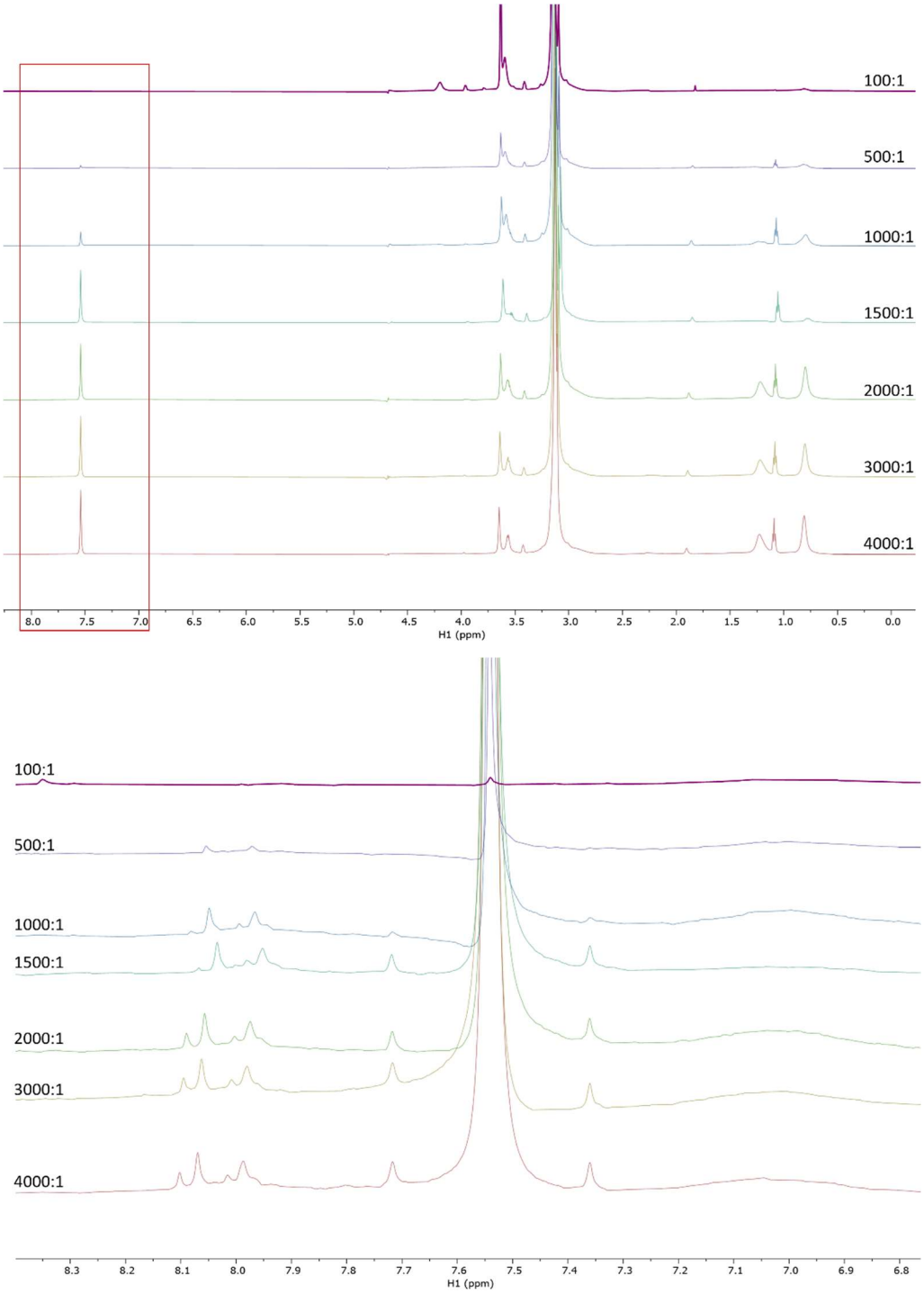

Figure 11. 1D ^{1}H spectra of 30.57±12.72 nm SMA-QA DMPC nanodisc with increasing amounts of cyclic hexapeptide c(WWWKKK). Ratios given are peptides per disc, and the disc is estimated to contain ~2000 lipid molecules. Top spectrum is the full spectrum (no peaks outside borders), while bottom spectrum is the range highlighted in red.

Conclusion

The cyclic AMPs studied in this work did not exhibit any significant conformational changes in different environments, ranging from water to micelles and phospholipid bilayers. From a method development perspective, the amount of high qualitative structural data that can be extracted rapidly diminish as the lipid model system gets more realistic and inevitably larger and more heterogenic. From phospholipid-based model systems like nanodiscs or liposomes we only expect to be able to extract chemical shifts, RDCs and RCSAs, where the latter requires partial alignment. This is complicated by the fact that AMPs are membrane active and are notorious for interfering with both phages and lipid systems in general. Initial results from SMA-QA nanodiscs in the presence of the studied AMPs however indicated that the integrity of the discs was not compromised by the AMP activity. That said, we did observe a decrease in alignment in the presence of AMPs, which will have to be considered.

The pilot experiments to explore the viability of using self-aligning SMA-QA nanodiscs as a model system suggests that there is a potentially viable concentration interval above the detection limit of ^{15}N-TROSY for ^{15}N labelled peptides, but at a healthily low peptide:lipid ratio. Because the model peptides provided for this work turned out to be conformationally featureless, investing in isotope labelling could not be justified and was thus deemed outside the scope of this work. At this point we conclude that the pilot study finds it viable to use self-aligning SMA-QA nanodiscs for conformational studies of small AMPs, but also that there are several difficulties associated with unordered interactions, exchange processes and saturation. The discs themselves need to be more thoroughly studied to map their behaviour and capacity under different conditions.

Experimental Section

NMR spectroscopy.

The synthesis of the peptides has been described previously.[68] c(WWWKKK), c(WKWKWK), c(WWWRRR), and c(WRWRWR) were dissolved in D_2O/H_2O 90:10 or pure d-DMSO (130 µL in 3 mm NMR tube, 600 µL in 5 mm NMR tube, or 120 µL in Shigemi tube; final sample concentration 2.5 mM). To obtain sample of SDS-micelle bound peptide (25 mM SDSd-25) a stock solution of SDS was added.[28]

NMR spectra were acquired on a Bruker Avance III HD spectrometer operating at 600 MHz for 1H, equipped with an inverse TCl cryo probe. All NMR spectra were acquired at 298 K using 5 mm tubes, except c(WWWRRR) in d-DMSO, which was acquired using a 3 mm Shigemi tube because of the limited amount of material. NOESY/ROESY, TOCSY, DQF-COSY, ^{15}N-HSQC, HSQC, HMBC, and H2BC NMR spectra were recorded with standard settings. NOESY and TOCSY spectra were recorded in water with mixing times of 100–400 ms and 80 ms, respectively. ROESY spectra were recorded in d-DMSO and SDSd-25 in water with mixing times of 25–200 ms.

Spectra were processed with TopSpin 3.6.0, and assignments were done manually.

NOE Buildup

The NOESY/ROESY spectra were imported into the Dynamics Center 2.8.3 NOE buildup toolbox under Method Center. Peaks were manually picked for their integrals and the buildup curves was reported in .pdf while the integrals were exported in .xlsx. The most isolated cross peak for the ortho aromatic protons on the Tryptophan furthest away from the diagonal was chosen as the internal reference at 2.46 Å distance.[34] All the cross peaks were registered, and the distances were given at the mixing time that had overall least outliers while being in the linear buildup phase, according to the .pdf file. Normally, 50 or 75 ms.

Structure calculation

Structure generation was performed with a standard simulated annealing (SA) protocol using X-PLOR 3.1 (NIH). An initial 25 structures were generated from which an average structure of the 10 lowest energy structures was produced as a starting point for a final SA round of 100 structures from which the top 10 lowest energy structures were selected. In all cases NOE derived distance constraints were used. The production protocol was repeated additionally with the inclusion of the experimentally derived coupling constants, as well as with the coupling constants and TALOS predicted dihedral angles.

Table 5. Summary of constraints used for structure generation.

WWWKKK			WWWRRR		
Water	DMSO	SDS	Water	DMSO	SDS

Intra-residue NOEs	34	10	31	25	25	17
Inter-residue NOEs	17	8	13	6	17	17
Of which are backbone	3	6	1	2	4	6
Ambiguous NOEs	31	60	32	36	63	25
Unassigned	17	47	51	25	24	6

The distances extracted from the NOE buildup were used as starting point for constructing the distance constraints for SA, with larger distances having more relaxed constraints using the first significant figure of the distance as a prompt, and up to the Van der Waals distance allowable. Constraints were optimised to relax any distance violations that arose during SA. This was done using the previously described SA protocol but with 10 structures and 25 structures generated in the initial and final SA steps.

Molecular dynamics calculations

The structures, c(WWWRRR) and c(WWWKKK), were constructed in Maestro (Schrödinger Release 2021–4: Maestro, Schrödinger, LLC, New York, NY, 2021), before TIP3P model water was added, and the topology and parameters was generated using CHARMM-GUI[86-88] solvation builder. The NAMD[89] software was used for simulations, with the systems being equilibrated in a periodic boundary box under NPT conditions up to 310K before the they were simulated for 100 ns under NVT conditions in 310K in water with 2fs simulation step. The geometry of the water was constrained used the SHAKE method and for pressure e control the Langevin piston method at 1atm with an oscillation period of 50fs and dampening scale of 25fs. Langevin dynamics was also used to control temperature at 310K with a dampening coefficient at $1ps^{-1}$, for long range electrostatic effects PME was used. New conformations were then found by calculating the RMSD value for each frame saved from the simulations and keeping the ones that had a difference higher than $2Å^2$. Calculating relative energies based on each conformation resulted then in the final conformation which were used in the simulation with the membrane models, one for each of the cyclic peptides.

Two membrane models were investigated, the first consisting of a DMPG/DMPC lipid combination and the second model consisting of POPG/POPE lipids. The first model consists

of 336 lipids, 319 DMPC lipids and 17 DMPG lipids, and the second consists of 170 lipids, 128 POPE lipids and 42 POPG lipids and they were both pre-equilibrated systems, the first by Sarre,[90] and the second by Hong.[91] Both membrane systems had NaCl ions added to both neutralize the membrane as well as ending up with a concentration of 0.15M in the solution itself before TIP3P water was added as additional solution around the system using VMD.[92]

As both the membranes and the cyclic peptides were already equilibrated, the equilibration was mainly focused on the water. This was done using NVT conditions with the peptide and membrane constrained before a general system equilibration in NPT conditions was conducted. The production simulations were in NPT conditions for 260ns with 2fs simulation step as well as the SHAKE method for the water and the previously explained method for temperature and pressure control.

Synthesis of SMA-QA

Following the procedure of Ravula *et al*.,[68, 74] (2-aminoethyl)trimethylammonium chloride hydrochloride (9.38 mmol, 1.3 g) was added to a solution of styrene maleic acid anhydride (SMA, 1g) in anhydrous DMF (5 mL), followed by trimethylamine (56.7 mmol, 5 mL) upon which the mixture took a dark yellow colour. The reaction mixture was stirred at 70°C for 2 hours, then cooled to room temperature, and precipitated with diethyl ether. The precipitate was washed 3 times with diethyl ether and dried *in vacuo*. The dried intermediate was dissolved in acetic anhydride (317 mmol, 30 mL), to which sodium acetate (8.05 mmol, 660 mg) and triethyl amine (1.98 mmol, 200 mg) were added. The reaction mixture was stirred at 80°C for 12 hours, cooled down, and precipitated in ether. The precipitate was washed 3 times in ether and dried *in vacuo*. The product was then dissolved in water and passed through a Sephadex LH-20 column. The product was collected and then lyophilised to give a crystalline brown powder and confirmed by IR stretching frequency shift from 1774 cm^{-1} to 1693 cm^{-1}.

Self-aligning nanodisc preparation

To a pear flask was added lipid (100 mg DMPC / 5.1 mg DMPG + 94.9 mg DMPC). Chloroform was added until all was dissolved. The solution was slowly evaporated on a rotavap at an angle for 1 hour to make a thin film. The film was then lyophilised overnight to get rid of trace amounts of chloroform. The film was diluted to a 20 mM solution by adding distilled water (7.15 mL). The solution was agitated with a pasteur pipette to make sure everything was dissolved and homogenous, then transferred to seven 1 mL eppendorf tubes. The tubes were freeze thawed three times by alternating between liquid nitrogen and hot water. The tubes were then stored in a freezer (-20^{O}C) until needed.

SMA-QA nanodiscs were prepared by adding a 100mg/mL SMA-QA stock to a final concentration depending on size goal (lipid:SMA-QA ratio of 1:1.5 for 10 nm discs; 1:1 for 20 nm discs; 1:0.25 for 30 nm discs). The combined SMA-QA and lipid mixture was incubated over night at room temperature and purified by SEC (Superdex 200 Increase 200/16 GL column operated on an AKTA purifier (GE Healthcare, Freiburg, Germany)). Fractions containing nanodiscs were combined and upconcentrated using centrifugation filters. Total lipid concentration was determined by ^{31}P NMR with 2 µL 5% Trymethyl Phosphate as internal reference. Nanodisc size was confirmed using a Malvern Zetasizer Nano ZS (Malvern Panalytical Ltd, Malvern, United Kingdom). The lipid/disc concentration was calculated according to equation (1).

$$\frac{lipid}{disc} = \frac{\pi(r_{Disc} - r_{SMA})^2}{A_{LHG}} \qquad (1)$$

where r_{Disc} is half the measured diameter of the nanodisc at 30°C, r_{SMA} is the width of the SMA polymer, and A_{LHG} is the reference value of the DMPC lipid head group at 30°C.

Author contributions: Conceptualisation: J.I. and F.G.R. Nanodisc preparation and NMR: F.G.R. Structure calculations: P.R. Data analysis: F.G.R., P.R., and J.I. Original draft: F.G.R. and J.I. Writing and editing: F.G.R., P.R., and J.I. Supervision: J.I.

Acknowledgements

Funding from the DigiBiotics project (Research Counsil of Norway, project ID 269425), the AntiBioSpec project of UiT the Arctic University of Norway (Cristin ID 20161326) and the NanoAMP project (Research Council of Norway, project ID 275186) is greatly appreciated.

References

(1) Hancock, R. E.; Lehrer, R. Cationic peptides: a new source of antibiotics. *Trends Biotechnol* **1998**, *16* (2), 82-88. DOI: S0167-7799(97)01156-6 [pii].
(2) Hancock, R. E. W.; Chapple, D. S. Peptide antibiotics. *Antimicrob Agents Ch* **1999**, *43* (6), 1317-1323.
(3) Zasloff, M. Antimicrobial peptides of multicellular organisms. *Nature* **2002**, *415* (6870), 389-395.
(4) Jenssen, H.; Hamill, P.; Hancock, R. E. W. Peptide antimicrobial agents. *Clin Microbiol Rev* **2006**, *19* (3), 491-+.
(5) Hancock, R. E. W. Peptide antibiotics. *Lancet* **1997**, *349* (9049), 418-422.
(6) Robbel, L.; Marahiel, M. A. Daptomycin, a bacterial lipopeptide synthesized by a nonribosomal machinery. *J. Biol. Chem.* **2010**, *285* (36), 27501-27508. DOI: 10.1074/jbc.R110.128181 From NLM Medline.
(7) Breukink, E.; de Kruijff, B. Lipid II as a target for antibiotics. *Nat Rev Drug Discov* **2006**, *5* (4), 321-332. DOI: 10.1038/nrd2004 From NLM Medline.
(8) Kupferwasser, L. I.; Skurray, R. A.; Brown, M. H.; Firth, N.; Yeaman, M. R.; Bayer, A. S. Plasmid-mediated resistance to thrombin-induced platelet microbicidal protein in staphylococci: role of the qacA locus. *Antimicrob. Agents Chemother.* **1999**, *43* (10), 2395-2399. DOI: 10.1128/AAC.43.10.2395 From NLM Medline.
(9) Li, Q.; Cebrian, R.; Montalban-Lopez, M.; Ren, H.; Wu, W.; Kuipers, O. P. Outer-membrane-acting peptides and lipid II-targeting antibiotics cooperatively kill Gram-negative pathogens. *Commun Biol* **2021**, *4* (1), 31. DOI: 10.1038/s42003-020-01511-1 From NLM Medline.
(10) Reddy, K. V.; Yedery, R. D.; Aranha, C. Antimicrobial peptides: premises and promises. *Int J Antimicrob Agents* **2004**, *24* (6), 536-547. DOI: 10.1016/j.ijantimicag.2004.09.005 From NLM Medline.
(11) Tanphaichitr, N.; Srakaew, N.; Alonzi, R.; Kiattiburut, W.; Kongmanas, K.; Zhi, R.; Li, W.; Baker, M.; Wang, G.; Hickling, D. Potential Use of Antimicrobial Peptides as Vaginal Spermicides/Microbicides. *Pharmaceuticals (Basel)* **2016**, *9* (1). DOI: 10.3390/ph9010013 From NLM PubMed-not-MEDLINE.
(12) Wang, X.; van Beekveld, R. A. M.; Xu, Y.; Parmar, A.; Das, S.; Singh, I.; Breukink, E. Analyzing mechanisms of action of antimicrobial peptides on bacterial membranes requires multiple complimentary assays and different bacterial strains. *Biochim Biophys Acta Biomembr* **2023**, *1865* (6), 184160. DOI: 10.1016/j.bbamem.2023.184160 From NLM Medline.
(13) Feng, S.; Liang, W.; Li, J.; Chen, Y.; Zhou, D.; Liang, L.; Lin, D.; Li, Y.; Zhao, H.; Du, H.; et al. MCR-1-dependent lipid remodelling compromises the viability of Gram-negative bacteria. *Emerg Microbes Infect* **2022**, *11* (1), 1236-1249. DOI: 10.1080/22221751.2022.2065934 From NLM Medline.
(14) Li, B.; Yin, F.; Zhao, X.; Guo, Y.; Wang, W.; Wang, P.; Zhu, H.; Yin, Y.; Wang, X. Colistin Resistance Gene mcr-1 Mediates Cell Permeability and Resistance to Hydrophobic Antibiotics. *Front Microbiol* **2019**, *10*, 3015. DOI: 10.3389/fmicb.2019.03015 From NLM PubMed-not-MEDLINE.
(15) Skov, R. L.; Monnet, D. L. Plasmid-mediated colistin resistance (mcr-1 gene): three months later, the story unfolds. *Euro Surveill* **2016**, *21* (9), 30155. DOI: 10.2807/1560-7917.ES.2016.21.9.30155.
(16) Birnbaum, J.; Kahan, F. M.; Kropp, H.; MacDonald, J. S. Carbapenems, a new class of beta-lactam antibiotics. Discovery and development of imipenem/cilastatin. *Am J Med* **1985**, *78* (6A), 3-21. DOI: 10.1016/0002-9343(85)90097-x From NLM Medline.
(17) Clarke, A. M.; Zemcov, S. J. Antibacterial activity of the cephamycin cefotetan: an in-vitro comparison with other beta-lactam antibiotics. *J. Antimicrob. Chemother.* **1983**, *11 Suppl*, 67-72. DOI: 10.1093/jac/11.suppl_a.67 From NLM Medline.
(18) D'Costa, V. M.; King, C. E.; Kalan, L.; Morar, M.; Sung, W. W.; Schwarz, C.; Froese, D.; Zazula, G.; Calmels, F.; Debruyne, R.; et al. Antibiotic resistance is ancient. *Nature* **2011**, *477* (7365), 457-461. DOI: 10.1038/nature10388 From NLM Medline.

(19) Hall, B. G.; Barlow, M. Evolution of the serine beta-lactamases: past, present and future. *Drug Resist Updat* **2004**, *7* (2), 111-123. DOI: 10.1016/j.drup.2004.02.003 From NLM Medline.
(20) Schneider, T.; Sahl, H. G. An oldie but a goodie - cell wall biosynthesis as antibiotic target pathway. *Int J Med Microbiol* **2010**, *300* (2-3), 161-169. DOI: 10.1016/j.ijmm.2009.10.005 From NLM Medline.
(21) Allen, M. M.; Yuen, C.; Medeiros, L.; Zizlsperger, N.; Farooq, M.; Kolodny, N. H. Effects of light and chloramphenicol stress on incorporation of nitrogen into cyanophycin in Synechocystis sp. strain PCC 6308. *Biochim. Biophys. Acta* **2005**, *1725* (2), 241-246. DOI: 10.1016/j.bbagen.2005.04.011 From NLM Medline.
(22) Perron, G. G.; Zasloff, M.; Bell, G. Experimental evolution of resistance to an antimicrobial peptide. *Proc Biol Sci* **2006**, *273* (1583), 251-256, Research Support, Non-U.S. Gov't. DOI: 10.1098/rspb.2005.3301.
(23) Wimley, W. C.; Hristova, K. Antimicrobial peptides: successes, challenges and unanswered questions. *J. Membr. Biol.* **2011**, *239* (1-2), 27-34. DOI: 10.1007/s00232-011-9343-0 From NLM Medline.
(24) Jean-Francois, F.; Elezgaray, J.; Berson, P.; Vacher, P.; Dufourc, E. J. Pore formation induced by an antimicrobial peptide: electrostatic effects. *Biophys. J.* **2008**, *95* (12), 5748-5756. DOI: 10.1529/biophysj.108.136655 From NLM Medline.
(25) Gazit, E.; Boman, A.; Boman, H. G.; Shai, Y. Interaction of the mammalian antibacterial peptide cecropin P1 with phospholipid vesicles. *Biochemistry* **1995**, *34* (36), 11479-11488. DOI: 10.1021/bi00036a021 From NLM Medline.
(26) Schmidt, N. W.; Wong, G. C. Antimicrobial peptides and induced membrane curvature: geometry, coordination chemistry, and molecular engineering. *Curr. Opin. Solid State Mater. Sci.* **2013**, *17* (4), 151-163. DOI: 10.1016/j.cossms.2013.09.004 From NLM PubMed-not-MEDLINE.
(27) Bechinger, B.; Lohner, K. Detergent-like actions of linear amphipathic cationic antimicrobial peptides. *Biochim. Biophys. Acta* **2006**, *1758* (9), 1529-1539. DOI: 10.1016/j.bbamem.2006.07.001 From NLM Medline.
(28) Appelt, C.; Wessolowski, A.; Soderhall, J. A.; Dathe, M.; Schmieder, P. Structure of the antimicrobial, cationic hexapeptide cyclo(RRWWRF) and its analogues in solution and bound to detergent micelles. *ChemBioChem* **2005**, *6* (9), 1654-1662. DOI: 10.1002/cbic.200500095 From NLM Medline.
(29) Roy, A.; Sarangi, N. K.; Ghosh, S.; Prabhakaran, A.; Keyes, T. E. Leaflet by Leaflet Synergistic Effects of Antimicrobial Peptides on Bacterial and Mammalian Membrane Models. *J Phys Chem Lett* **2023**, *14* (16), 3920-3928. DOI: 10.1021/acs.jpclett.3c00119 From NLM Medline.
(30) Avci, F. G.; Akbulut, B. S.; Ozkirimli, E. Membrane Active Peptides and Their Biophysical Characterization. *Biomolecules* **2018**, *8* (3). DOI: 10.3390/biom8030077 From NLM Medline.
(31) Hadjicharalambous, A.; Bournakas, N.; Newman, H.; Skynner, M. J.; Beswick, P. Antimicrobial and Cell-Penetrating Peptides: Understanding Penetration for the Design of Novel Conjugate Antibiotics. *Antibiotics (Basel)* **2022**, *11* (11). DOI: 10.3390/antibiotics11111636 From NLM PubMed-not-MEDLINE.
(32) Wojciechowska, M.; Miszkiewicz, J.; Trylska, J. Conformational Changes of Anoplin, W-MreB(1-9), and (KFF)(3)K Peptides near the Membranes. *Int J Mol Sci* **2020**, *21* (24). DOI: 10.3390/ijms21249672 From NLM Medline.
(33) Eiriksdottir, E.; Konate, K.; Langel, U.; Divita, G.; Deshayes, S. Secondary structure of cell-penetrating peptides controls membrane interaction and insertion. *Biochim. Biophys. Acta* **2010**, *1798* (6), 1119-1128. DOI: 10.1016/j.bbamem.2010.03.005 From NLM Medline.
(34) Claridge, T. D. W. *High-Resolution NMR Techniques*; Elsevier, 2016.
(35) Ramsey, N. F. Electron Coupled Interactions between Nuclear Spins in Molecules. *Physical Review* **1953**, *91* (2), 303-307. DOI: 10.1103/PhysRev.91.303.
(36) Ramsey, N. F.; Purcell, E. M. Interactions between Nuclear Spins in Molecules. *Physical Review* **1952**, *85* (1), 143-144. DOI: 10.1103/PhysRev.85.143.

(37) Farina, B.; Del Gatto, A.; Comegna, D.; Di Gaetano, S.; Capasso, D.; Isernia, C.; Saviano, M.; Fattorusso, R.; Zaccaro, L.; Russo, L. Conformational studies of RGDechi peptide by natural-abundance NMR spectroscopy. *J. Pept. Sci.* **2019**, *25* (5), e3166. DOI: 10.1002/psc.3166 From NLM Medline.
(38) Wishart, D. S.; Case, D. A. Use of chemical shifts in macromolecular structure determination. *Methods Enzymol.* **2001**, *338*, 3-34. DOI: 10.1016/s0076-6879(02)38214-4 From NLM Medline.
(39) Wishart, D. S.; Nip, A. M. Protein chemical shift analysis: a practical guide. *Biochem. Cell Biol.* **1998**, *76* (2-3), 153-163. DOI: 10.1139/bcb-76-2-3-153 From NLM Medline.
(40) Wishart, D. S.; Sykes, B. D. Chemical shifts as a tool for structure determination. *Methods Enzymol.* **1994**, *239*, 363-392. DOI: 10.1016/s0076-6879(94)39014-2 From NLM Medline.
(41) Wishart, D. S.; Sykes, B. D.; Richards, F. M. The chemical shift index: a fast and simple method for the assignment of protein secondary structure through NMR spectroscopy. *Biochemistry* **1992**, *31* (6), 1647-1651. DOI: 10.1021/bi00121a010 From NLM Medline.
(42) Schwarzinger, S.; Kroon, G. J.; Foss, T. R.; Chung, J.; Wright, P. E.; Dyson, H. J. Sequence-dependent correction of random coil NMR chemical shifts. *J. Am. Chem. Soc.* **2001**, *123* (13), 2970-2978. DOI: 10.1021/ja003760i From NLM Medline.
(43) Ting, D.; Wang, G.; Shapovalov, M.; Mitra, R.; Jordan, M. I.; Dunbrack, R. L., Jr. Neighbor-dependent Ramachandran probability distributions of amino acids developed from a hierarchical Dirichlet process model. *PLoS Comput Biol* **2010**, *6* (4), e1000763. DOI: 10.1371/journal.pcbi.1000763 From NLM Medline.
(44) Tamiola, K.; Acar, B.; Mulder, F. A. Sequence-specific random coil chemical shifts of intrinsically disordered proteins. *J. Am. Chem. Soc.* **2010**, *132* (51), 18000-18003. DOI: 10.1021/ja105656t From NLM Medline.
(45) Tamiola, K.; Mulder, F. A. Using NMR chemical shifts to calculate the propensity for structural order and disorder in proteins. *Biochem. Soc. Trans.* **2012**, *40* (5), 1014-1020. DOI: 10.1042/BST20120171 From NLM Medline.
(46) Dinku, W.; Isaksson, J.; Rylandsholm, F. G.; Bour, P.; Brichtová, E.; Choi, S. U.; Lee, S. H.; Jung, Y. S.; No, Z. S.; Svendsen, J. S. M.; et al. Anti-proliferative activity of a novel tricyclic triterpenoid acid from resin against four human cancer cell lines. *Applied Biological Chemistry* **2020**, *63* (1). DOI: 10.1186/s13765-020-00499-w.
(47) Sarfati, M.; Courtieu, J.; Lesot, P. First successful enantiomeric discrimination of chiral alkanes using NMR spectroscopy. *Chem. Commun.* **2000**, (13), 1113-1114. DOI: 10.1039/b002806l.
(48) Thiele, C. M. Simultaneous assignment of all diastereotopic protons in strychnine using RDCs: PELG as alignment medium for organic molecules. *J. Org. Chem.* **2004**, *69* (22), 7403-7413. DOI: 10.1021/jo049867w From NLM Medline.
(49) Thiele, C. M.; Berger, S. Probing the diastereotopicity of methylene protons in strychnine using residual dipolar couplings. *Org. Lett.* **2003**, *5* (5), 705-708. DOI: 10.1021/ol0275163 From NLM PubMed-not-MEDLINE.
(50) Meyer, N. C.; Krupp, A.; Schmidts, V.; Thiele, C. M.; Reggelin, M. Polyacetylenes as enantiodifferentiating alignment media. *Angew. Chem. Int. Ed. Engl.* **2012**, *51* (33), 8334-8338. DOI: 10.1002/anie.201201891 From NLM Medline.
(51) Marx, A.; Schmidts, V.; Thiele, C. M. How different are diastereomorphous orientations of enantiomers in the liquid crystalline phases of PBLG and PBDG: a case study. *Magn. Reson. Chem.* **2009**, *47* (9), 734-740. DOI: 10.1002/mrc.2454 From NLM Medline.
(52) Montag, T.; Thiele, C. M. Cross-linked helically chiral poly-(gamma-benzyl-L-glutamate) as enantiodiscriminating alignment medium. *Chemistry* **2013**, *19* (7), 2271-2274. DOI: 10.1002/chem.201202554 From NLM Medline.
(53) Krupp, A.; Reggelin, M. Phenylalanine-based polyarylacetylenes as enantiomer-differentiating alignment media. *Magn. Reson. Chem.* **2012**, *50 Suppl 1*, S45-52. DOI: 10.1002/mrc.3894 From NLM Medline.

(54) Luy, B.; Kobzar, K.; Kessler, H. An easy and scalable method for the partial alignment of organic molecules for measuring residual dipolar couplings. *Angew. Chem. Int. Ed. Engl.* **2004**, *43* (9), 1092-1094. DOI: 10.1002/anie.200352860 From NLM PubMed-not-MEDLINE.
(55) Gayathri, C.; Tsarevsky, N. V.; Gil, R. R. Residual dipolar couplings (RDCs) analysis of small molecules made easy: fast and tuneable alignment by reversible compression/relaxation of reusable PMMA Gels. *Chemistry* **2010**, *16* (12), 3622-3626. DOI: 10.1002/chem.200903378 From NLM PubMed-not-MEDLINE.
(56) Luy, B.; Kobzar, K.; Knor, S.; Furrer, J.; Heckmann, D.; Kessler, H. Orientational properties of stretched polystyrene gels in organic solvents and the suppression of their residual 1H NMR signals. *J. Am. Chem. Soc.* **2005**, *127* (17), 6459-6465. DOI: 10.1021/ja043344o From NLM PubMed-not-MEDLINE.
(57) Freudenberger, J. C.; Spiteller, P.; Bauer, R.; Kessler, H.; Luy, B. Stretched poly(dimethylsiloxane) gels as NMR alignment media for apolar and weakly polar organic solvents: an ideal tool for measuring RDCs at low molecular concentrations. *J. Am. Chem. Soc.* **2004**, *126* (45), 14690-14691. DOI: 10.1021/ja046155e From NLM Medline.
(58) Kobzar, K.; Kessler, H.; Luy, B. Stretched gelatin gels as chiral alignment media for the discrimination of enantiomers by NMR spectroscopy. *Angew. Chem. Int. Ed. Engl.* **2005**, *44* (20), 3145-3147. DOI: 10.1002/anie.200462736 From NLM PubMed-not-MEDLINE.
(59) Marx, A.; Thiele, C. Orientational properties of poly-gamma-benzyl-L-glutamate: influence of molecular weight and solvent on order parameters of the solute. *Chemistry* **2009**, *15* (1), 254-260. DOI: 10.1002/chem.200801147 From NLM PubMed-not-MEDLINE.
(60) Liu, Y.; Navarro-Vazquez, A.; Gil, R. R.; Griesinger, C.; Martin, G. E.; Williamson, R. T. Application of anisotropic NMR parameters to the confirmation of molecular structure. *Nat Protoc* **2019**, *14* (1), 217-247. DOI: 10.1038/s41596-018-0091-9.
(61) Schmidt, M.; Sun, H.; Leonov, A.; Griesinger, C.; Reinscheid, U. M. Chiral discrimination of amines by anisotropic NMR parameters using chiral polyacrylamide-based gels. *Magn. Reson. Chem.* **2012**, *50 Suppl 1*, S38-44. DOI: 10.1002/mrc.3886 From NLM Medline.
(62) Kummerlöwe, G.; Kiran, M. U.; Luy, B. Covalently cross-linked gelatin allows chiral distinction at elevated temperatures and in DMSO. *Chemistry* **2009**, *15* (45), 12192-12195. DOI: 10.1002/chem.200902193 From NLM Medline.
(63) Buchler, S. S.; Kummerlöwe, G.; Luy, B. Naturally occurring biodegradable polymers as the basis of chiral gels for the distinction of enantiomers by partially oriented NMR spectroscopy. *Int J Artif Organs* **2011**, *34* (2), 134-138. DOI: 10.5301/ijao.2011.6419 From NLM Medline.
(64) Pracht, P.; Bohle, F.; Grimme, S. Automated exploration of the low-energy chemical space with fast quantum chemical methods. *Phys. Chem. Chem. Phys.* **2020**, *22* (14), 7169-7192. DOI: 10.1039/c9cp06869d From NLM PubMed-not-MEDLINE.
(65) Barone, V.; Cossi, M. Quantum Calculation of Molecular Energies and Energy Gradients in Solution by a Conductor Solvent Model. *The Journal of Physical Chemistry A* **1998**, *102* (11), 1995-2001. DOI: 10.1021/jp9716997.
(66) Cossi, M.; Rega, N.; Scalmani, G.; Barone, V. Energies, structures, and electronic properties of molecules in solution with the C-PCM solvation model. *J. Comput. Chem.* **2003**, *24* (6), 669-681. DOI: 10.1002/jcc.10189 From NLM PubMed-not-MEDLINE.
(67) Jiang, F.; Geng, H. Computational Methods for Studying Conformational Behaviors of Cyclic Peptides. *Methods Mol Biol* **2019**, *2001*, 61-71. DOI: 10.1007/978-1-4939-9504-2_4 From NLM Medline.
(68) Rainsford, P.; Rylandsholm, F. G.; Jakubec, M.; Silk, M.; Juskewitz, E.; Ericson, J. U.; Svendsen, J. S.; Engh, R. A.; Isaksson, J. Label-free measurement of antimicrobial peptide interactions with lipid vesicles and nanodiscs using microscale thermophoresis. *Sci Rep* **2023**, *13* (1), 12619. DOI: 10.1038/s41598-023-39785-0 From NLM Medline.
(69) Jakubec, M.; Rylandsholm, F. G.; Rainsford, P.; Silk, M.; Bril'kov, M.; Kristoffersen, T.; Juskewitz, E.; Ericson, J. U.; Svendsen, J. S. M. Goldilocks Dilemma: LPS Works Both as the Initial Target and a

Barrier for the Antimicrobial Action of Cationic AMPs on E. coli. *Biomolecules* **2023**, *13* (7). DOI: 10.3390/biom13071155.
(70) Eikås, K. D. R.; Rylandsholm, F. G.; Kristoffersen, T.; Jakubec, M.; Silk, M. R.; Svendsen, J. S. M.; Isaksson, J.; Ruud, K.; Krupová, M. Conformational Studies of Cyclic Hexapeptides with Vibrational Circular Dichroism and Nuclear Magnetic Resonance. .
(71) Wüthrich, K. *NMR of Proteins and Nucleic Acids*; Wiley, 1986.
(72) Appelt, C.; Wessolowski, A.; Dathe, M.; Schmieder, P. Structures of cyclic, antimicrobial peptides in a membrane-mimicking environment define requirements for activity. *J. Pept. Sci.* **2008**, *14* (4), 524-527. DOI: 10.1002/psc.924 From NLM Medline.
(73) Ravula, T.; Ramadugu, S. K.; Di Mauro, G.; Ramamoorthy, A. Bioinspired, Size-Tunable Self-Assembly of Polymer-Lipid Bilayer Nanodiscs. *Angew. Chem. Int. Ed. Engl.* **2017**, *56* (38), 11466-11470. DOI: 10.1002/anie.201705569.
(74) Ravula, T.; Hardin, N. Z.; Ramadugu, S. K.; Cox, S. J.; Ramamoorthy, A. Formation of pH-Resistant Monodispersed Polymer-Lipid Nanodiscs. *Angew. Chem. Int. Ed. Engl.* **2018**, *57* (5), 1342-1345. DOI: 10.1002/anie.201712017.
(75) Ravula, T.; Hardin, N. Z.; Ramamoorthy, A. Polymer nanodiscs: Advantages and limitations. *Chem. Phys. Lipids* **2019**, *219*, 45-49. DOI: 10.1016/j.chemphyslip.2019.01.010.
(76) Ravula, T.; Ramamoorthy, A. Magnetic Alignment of Polymer Macro-Nanodiscs Enables Residual-Dipolar-Coupling-Based High-Resolution Structural Studies by NMR Spectroscopy. *Angew. Chem. Int. Ed. Engl.* **2019**, *58* (42), 14925-14928. DOI: 10.1002/anie.201907655.
(77) Stangl, M.; Veerappan, A.; Kroeger, A.; Vogel, P.; Schneider, D. Detergent properties influence the stability of the glycophorin A transmembrane helix dimer in lysophosphatidylcholine micelles. *Biophys. J.* **2012**, *103* (12), 2455-2464. DOI: 10.1016/j.bpj.2012.11.004 From NLM Medline.
(78) Gu, H.; Kato, T.; Kumeta, H.; Kumaki, Y.; Tsukamoto, T.; Kikukawa, T.; Demura, M.; Ishida, H.; Vogel, H. J.; Aizawa, T. Three-Dimensional Structure of the Antimicrobial Peptide Cecropin P1 in Dodecylphosphocholine Micelles and the Role of the C-Terminal Residues. *ACS Omega* **2022**, *7* (36), 31924-31934. DOI: 10.1021/acsomega.2c02778 From NLM PubMed-not-MEDLINE.
(79) Terakawa, M. S.; Lin, Y.; Kinoshita, M.; Kanemura, S.; Itoh, D.; Sugiki, T.; Okumura, M.; Ramamoorthy, A.; Lee, Y. H. Impact of membrane curvature on amyloid aggregation. *Biochim Biophys Acta Biomembr* **2018**, *1860* (9), 1741-1764. DOI: 10.1016/j.bbamem.2018.04.012 From NLM PubMed-not-MEDLINE.
(80) Stepien, P.; Augustyn, B.; Poojari, C.; Galan, W.; Polit, A.; Vattulainen, I.; Wisnieska-Becker, A.; Rog, T. Complexity of seemingly simple lipid nanodiscs. *Biochim Biophys Acta Biomembr* **2020**, *1862* (11), 183420. DOI: 10.1016/j.bbamem.2020.183420 From NLM Medline.
(81) Bibow, S.; Carneiro, M. G.; Sabo, T. M.; Schwiegk, C.; Becker, S.; Riek, R.; Lee, D. Measuring membrane protein bond orientations in nanodiscs via residual dipolar couplings. *Protein Sci.* **2014**, *23* (7), 851-856. DOI: 10.1002/pro.2482 From NLM Medline.
(82) Kučerka, N.; Liu, Y.; Chu, N.; Petrache, H. I.; Tristram-Nagle, S.; Nagle, J. F. Structure of Fully Hydrated Fluid Phase DMPC and DLPC Lipid Bilayers Using X-Ray Scattering from Oriented Multilamellar Arrays and from Unilamellar Vesicles. *Biophys. J.* **2005**, *88* (4), 2626-2637. DOI: 10.1529/biophysj.104.056606.
(83) Hu, M.; de Jong, D. H.; Marrink, S. J.; Deserno, M. Gaussian curvature elasticity determined from global shape transformations and local stress distributions: a comparative study using the MARTINI model. *Faraday Discuss.* **2013**, *161*, 365-382; discussion 419-359. DOI: 10.1039/c2fd20087b From NLM Medline.
(84) Marsh, D. *Handbook of Lipid Bilayers*; CRC Press, 2013.
(85) Dorr, J. M.; Scheidelaar, S.; Koorengevel, M. C.; Dominguez, J. J.; Schafer, M.; van Walree, C. A.; Killian, J. A. The styrene-maleic acid copolymer: a versatile tool in membrane research. *Eur Biophys J* **2016**, *45* (1), 3-21. DOI: 10.1007/s00249-015-1093-y From NLM Medline.
(86) Huang, J.; MacKerell, A. D., Jr. CHARMM36 all-atom additive protein force field: validation based on comparison to NMR data. *J. Comput. Chem.* **2013**, *34* (25), 2135-2145. DOI: 10.1002/jcc.23354 From NLM Medline.

(87) Jo, S.; Kim, T.; Iyer, V. G.; Im, W. CHARMM-GUI: a web-based graphical user interface for CHARMM. *J. Comput. Chem.* **2008**, *29* (11), 1859-1865. DOI: 10.1002/jcc.20945 From NLM Medline.
(88) Lee, J.; Cheng, X.; Swails, J. M.; Yeom, M. S.; Eastman, P. K.; Lemkul, J. A.; Wei, S.; Buckner, J.; Jeong, J. C.; Qi, Y.; et al. CHARMM-GUI Input Generator for NAMD, GROMACS, AMBER, OpenMM, and CHARMM/OpenMM Simulations Using the CHARMM36 Additive Force Field. *J Chem Theory Comput* **2016**, *12* (1), 405-413. DOI: 10.1021/acs.jctc.5b00935 From NLM Medline.
(89) Phillips, J. C.; Hardy, D. J.; Maia, J. D. C.; Stone, J. E.; Ribeiro, J. V.; Bernardi, R. C.; Buch, R.; Fiorin, G.; Henin, J.; Jiang, W.; et al. Scalable molecular dynamics on CPU and GPU architectures with NAMD. *J. Chem. Phys.* **2020**, *153* (4), 044130. DOI: 10.1063/5.0014475 From NLM PubMed-not-MEDLINE.
(90) Rainsford, P.; Sarre, B. R.; Falavigna, M.; Brandsdal, B. O.; Flaten, G. E.; Jakubec, M.; Isaksson, J. WIND-PVPA: Water/Ion NMR Detected PVPA to assess lipid barrier integrity in vitro through quantification of passive water- and ion transport. *Biochim Biophys Acta Biomembr* **2022**, *1864* (7), 183911. DOI: 10.1016/j.bbamem.2022.183911 From NLM Medline.
(91) Hong, C.; Tieleman, D. P.; Wang, Y. Microsecond molecular dynamics simulations of lipid mixing. *Langmuir* **2014**, *30* (40), 11993-12001. DOI: 10.1021/la502363b From NLM Medline.
(92) Humphrey, W.; Dalke, A.; Schulten, K. VMD: visual molecular dynamics. *J Mol Graph* **1996**, *14* (1), 33-38, 27-38. DOI: 10.1016/0263-7855(96)00018-5 From NLM Medline.

Supporting information

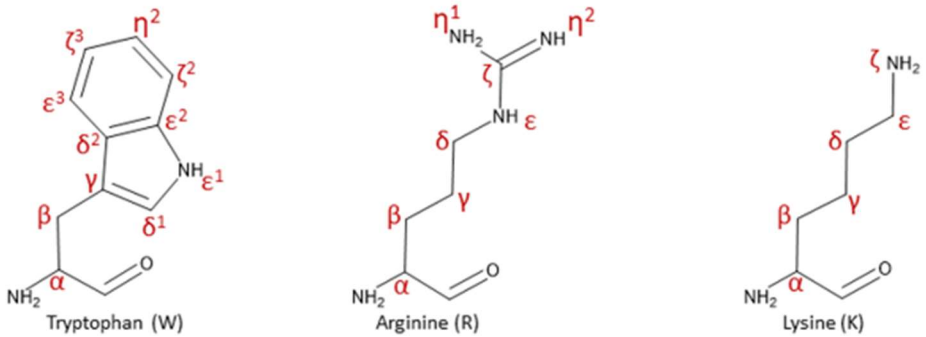

Figure S 1. Numbering of atoms on amino acids sidechains with Greek letters.

The chemical shifts of the four cyclic hexapeptides in water are already published,[69] but they are added in the Supporting information for convenience.

Table S1. Full assignment of c(WWWKKK) in water.

c(WWWKKK)														
Residue #	Amino acid	Chemical shift (δ)												
1	W - Tryptophan	NHα	CO	α	β	ε1	δ1	γ	δ2	ε3	ζ3	η2	ζ2	ε2
	^{1}H	7.85		4.48	2.99/2.86	10.10	7.06			7.46	7.09	7.17	7.41	
	^{13}C/^{15}N	118.01	173.41	54.70	26.00	129.28	124.45	108.96	127.01	118.48	119.41	122.04	111.98	136.34
2	W - Tryptophan	NHα	CO	α	β	ε1	δ1	γ	δ2	ε3	ζ3	η2	ζ2	ε2
	^{1}H	7.33		4.51	3.11/2.87	10.05	6.95			7.30	7.05	7.15	7.39	
	^{13}C/^{15}N	119.00	172.67	54.55	26.36	130.00	124.76	108.30	127.06	118.30	119.59	122.16	112.04	136.20
3	W - Tryptophan	NHα	CO	α	β	ε1	δ1	γ	δ2	ε3	ζ3	η2	ζ2	ε2
	^{1}H	7.55		4.45	3.06/2.76	10.07	6.92			7.30	7.02	7.11	7.33	
	^{13}C/^{15}N	121.25	172.67	55.19	26.06	129.56	124.19	108.54	126.86	118.30	119.44	122.05	111.94	136.24
4	K -Lysine	NHα	CO	α	β	γ	δ	ε	ζ					
	^{1}H	7.84		3.75	1.49/1.67	0.66	1.30/1.58	2.26	7.41					
	^{13}C/^{15}N	120.75	173.08	54.90	30.07	21.86	26.19	39.24	96.51					
5	K -Lysine	NHα	CO	α	β	γ	δ	ε	ζ					
	^{1}H	8.03		4.10	1.51	1.68/1.50	1.32/1.24	2.88	7.46					
	^{13}C/^{15}N	119.47	173.29	53.60	28.83	30.06	22.34	39.43	96.73					
6	K -Lysine	NHα	CO	α	β	γ	δ	ε	ζ					
	^{1}H	7.77		3.88	1.22	0.85/0.74	1.33	2.61	7.37					
	^{13}C/^{15}N	119.35	173.76	54.55	29.43	21.86		39.24	96.52					

Table S2. Full assignment of c(WKWKWK) in water.

c(WKWKWK)													
Residue #	Amino acid	Chemical shift (δ)											
1	W - Tryptophan	NHα	CO	α	β	ε1	δ1	γ	δ2	ε3	ζ3	η2	ζ2	ε2
	^{1}H	7.99		4.54	3.09	10.17	7.16			7.52	7.10	7.17	7.37	
	^{13}C/^{15}N	119.292	173.01	54.66	25.99	129.67	124.35	108.77	127.06	118.37	119.46	122.03	112.04	136.21
2	K -Lysine	NHα	CO	α	β	γ	δ	ε	ζ					
	^{1}H	7.62		3.89	1.42	0.67	1.28	2.55	7.35					
	^{13}C/^{15}N	120.24	172.91	54.55	29.59	21.59	26.21	39.25	134.12/95.83					

Table S3. Full assignment of c(WRWRWR) in water.

c(WRWRWR)														
Residue #	Amino acid	Chemical shift (δ)												
1	W - Tryptophan	NHα	CO	α	β	ε1	δ1	γ	δ2	ε3	ζ3	η2	ζ2	ε2
	^{1}H	8.07		4.54	3.13	10.13	7.16			7.53	7.10	7.16	7.37	
	^{13}C/^{15}N	119.43	172.84	54.84	26.04	129.65	124.44	108.78	126.96	118.23	119.39	122.07	111.97	136.23
2	R - Arginine	NHα	CO	α	β	γ	δ	ε	ζ	η1	η2			
	^{1}H	7.65		3.90	1.41	0.82	2.71	6.77						
	^{13}C/^{15}N	119.96	172.88	54.39	27.28	23.71	40.44	84.78	153.71					

Table S4. Full assignment of c(WWWRRR) in water.

c(WWWRRR)

Residue #	Amino acid	Chemical shift (δ)												
1	W - Tryptophan	NHα	CO	α	β	ε1	δ1	γ	δ2	ε3	ζ3	η2	ζ2	ε2
	^{1}H	7.88		4.52	2.85/3.04	10.03	7.04			7.46	7.07	7.15	7.38	
	^{13}C/^{15}N	118.00	173.20	54.68	26.04	129.05	124.44	109.20	126.79	118.31	119.29	122.02	111.89	136.27
2	W - Tryptophan	NHα	CO	α	β	ε1	δ1	γ	δ2	ε3	ζ3	η2	ζ2	ε2
	^{1}H	7.42		4.54	2.98/3.03	10.05	7.02			7.38	7.08	7.16	7.40	
	^{13}C/^{15}N	119.05	172.55	54.36	26.68	130.00	124.76	108.40	127.37	118.30	119.44	122.03	112.02	136.22
3	W - Tryptophan	NHα	CO	α	β	ε1	δ1	γ	δ2	ε3	ζ3	η2	ζ2	ε2
	^{1}H	7.64		4.43	2.85/3.05	10.03	6.94			7.36	7.04	7.12	7.33	
	^{13}C/^{15}N	121.23	173.10	55.49	26.04	129.50	124.27	108.40	126.82	118.17	119.34	122.03	111.87	136.23
4	R - Arginine	NHα	CO	α	β	γ	δ	ε	ζ	η1	η2			
	^{1}H	7.94		3.72	1.58/1.50	0.74/0.87	2.75/2.73	6.77						
	^{13}C/^{15}N	120.23	172.89	54.85	26.37	24.11	40.38	85.03	156.63					
5	R - Arginine	NHα	CO	α	β	γ	δ	ε	ζ	η1	η2			
	^{1}H	8.15		4.18	1.48/1.75	1.49	3.11	7.12						
	^{13}C/^{15}N	119.02	172.78	53.24	27.98	24.43	40.54	84.97	156.89					
6	R - Arginine	NHα	CO	α	β	γ	δ	ε	ζ	η1	η2			
	^{1}H	7.87		3.85	1.29/1.24	0.85/0.93	2.78/2.72	6.80						
	^{13}C/^{15}N	119.50	173.54	54.83	27.01	23.76	40.21	84.97	156.57					

Table S5. Full assignment of c(WWWKKK) in DMSO.

c(WWWKKK)														
Residue #	Amino acid	Chemical shift (δ)												
1	W - Tryptophan	NHα	CO	α	β	ε1	δ1	γ	δ2					
	^{1}H	8.07		4.23	3.11/3.27	10.84	7.10			7.57	6.99	7.09	7.35	
	$^{13C}/^{15N}$	116.17	171.17	55.38	26.78	131.28	123.95	110.71	127.63	118.34	118.79	121.45	111.88	136.55
2	W - Tryptophan	NHα	CO	α	β	ε1	δ1	γ	δ2					
	^{1}H	7.94		4.31	3.03/3.11	10.80	7.06			7.51	6.98	7.08	7.34	
	$^{13C}/^{15N}$	116.96	171.36	55.17	27.41	131.12	124.10	110.92	127.68	118.69	118.79	121.45	111.88	136.63
3	W - Tryptophan	NHα	CO	α	β	ε1	δ1	γ	δ2					
	^{1}H	8.20		4.31	3.11/3.28	10.81	7.06			7.51	6.98	7.08	7.34	
	$^{13C}/^{15N}$	118.75	171.36	55.86	27.00	131.12	123.81	110.60	127.66	118.69	118.79	121.45	111.88	136.59
4	K -Lysine	NHα	CO	α	β	γ	δ	ε	ζ					
	^{1}H	8.21		3.94	1.74/1.79	1.15	1.47	2.68	7.66					
	$^{13C}/^{15N}$	116.67		54.38	30.23	22.99	22.98	39.16	133.24					
5	K -Lysine	NHα	CO	α	β	γ	δ	ε	ζ					
	^{1}H	8.00		4.12	1.72/1.78	1.32/1.38	1.55	2.76	7.67					
	$^{13C}/^{15N}$	115.23	171.82	53.45	30.87	22.75	22.71	39.27	133.24					
6	K -Lysine	NHα	CO	α	β	γ	δ	ε	ζ					
	^{1}H	8.03		3.87	1.55	0.98/1.12	1.39	2.59	7.67					
	$^{13C}/^{15N}$	116.56	171.55	54.54	30.58	22.62	22.74	39.08	133.24					

Table S6. Full assignment of c(WKWKWK) in DMSO.

c(WKWKWK)														
Residue #	Amino acid	Chemical shift (δ)												
1	W - Tryptophan	NHα	CO	α	β	ε1	δ1	γ	δ2	ε3	ζ3	η2	ζ2	ε2
	^{1}H	8.15		4.37	3.16/3.25	10.85	7.17			7.58	7.00	7.08	7.35	
	$^{13C}/_{15N}$	117.10	171.58	55.20	27.11	131.24	123.92	110.70	127.65	118.84	118.84	121.48	111.83	136.40
2	K -Lysine	NHα	CO	α	β	γ	δ	ε	ζ					
	^{1}H	8.03		3.89	1.60	1.00	1.38	2.58						
	$^{13C}/_{15N}$	116.70	171.44	54.41	30.56	22.69	27.12	39.13						
3	W - Tryptophan	NHα	CO	α	β	ε1	δ1	γ	δ2	ε3	ζ3	η2	ζ2	ε2
	1H	8.15		4.37	3.16/3.25	10.85	7.17			7.58	7.00	7.08	7.35	
	13C/15N	117.10	171.58	55.20	27.11	131.24	123.92	110.70	127.65	118.84	118.84	121.48	111.83	136.40
4	K -Lysine	NHα	CO	α	β	γ	δ	ε	ζ					
	1H	8.03		3.89	1.60	1.00	1.38	2.58						
	13C/15N	116.70	171.44	54.41	30.56	22.69	27.12	39.13						
5	W - Tryptophan	NHα	CO	α	β	ε1	δ1	γ	δ2	ε3	ζ3	η2	ζ2	ε2
	1H	8.15		4.37	3.16/3.25	10.85	7.17			7.58	7.00	7.08	7.35	
	13C/15N	117.10	171.58	55.20	27.11	131.24	123.92	110.70	127.65	118.84	118.84	121.48	111.83	136.40
6	K -Lysine	NHα	CO	α	β	γ	δ	ε	ζ					
	1H	8.03		3.89	1.60	1.00	1.38	2.58						
	13C/15N	116.70	171.44	54.41	30.56	22.69	27.12	39.13						

Table S7. Full assignment of c(WRWRWR) in DMSO.

c(WRWRWR)														
Residue #	Amino acid	Chemical shift (δ)												
1	W - Tryptophan	NHα	CO	α	β	ε1	δ1	γ	δ2	ε3	ζ3	η2	ζ2	ε2
	^{1}H	8.15		4.36	3.18/3.27	10.78	7.16			7.57	7.00	7.08	7.35	
	$^{13C}/^{15N}$	116.85	171.46	55.26	27.11	131.07	123.91	110.68	127.60	118.75	118.86	121.53	111.89	136.68
2	R - Arginine	NHα	CO	α	β	γ	δ	ε	ζ	η1	η2			
	^{1}H	8.11		3.94	1.57/1.70	1.26/1.29	2.98	7.45						
	$^{13C}/^{15N}$	116.92	171.54	54.04	28.27	25.36	40.79	84.97	157.22					
3	W - Tryptophan	NHα	CO	α	β	ε1	δ1	γ	δ2	ε3	ζ3	η2	ζ2	ε2
	1H	8.15		4.36	3.18/3.27	10.78	7.16			7.57	7.00	7.08	7.35	
	13C/15N	116.85	171.46	55.26	27.11	131.07	123.91	110.68	127.60	118.75	118.86	121.53	111.89	136.68
4	R - Arginine	NHα	CO	α	β	γ	δ	ε	ζ	η1	η2			
	1H	8.11		3.94	1.57/1.70	1.26/1.29	2.98	7.45						
	13C/15N	116.92	171.54	54.04	28.27	25.36	40.79	84.97	157.22					
5	W - Tryptophan	NHα	CO	α	β	ε1	δ1	γ	δ2	ε3	ζ3	η2	ζ2	ε2
	1H	8.15		4.36	3.18/3.27	10.78	7.16			7.57	7.00	7.08	7.35	
	13C/15N	116.85	171.46	55.26	27.11	131.07	123.91	110.68	127.60	118.75	118.86	121.53	111.89	136.68
6	R - Arginine	NHα	CO	α	β	γ	δ	ε	ζ	η1	η2			
	1H	8.11		3.94	1.57/1.70	1.26/1.29	2.98	7.45						
	13C/15N	116.92	171.54	54.04	28.27	25.36	40.79	84.97	157.22					

Table S8. Full assignment of c(WWWRRR) in DMSO.

c(WWWRRR)														
Residue #	Amino acid	Chemical shift (δ)												
1	W - Tryptophan	NHα	CO	α	β	ε1	δ1	γ	δ2	ε3	ζ3	η2	ζ2	ε2
	^{1}H	8.04		4.27	2.99/3.08	10.76	7.04			7.52	6.97	7.07	7.34	
	$^{13C}/^{15N}$	116.61	171.27	55.27	27.16	130.99	123.81	110.76	127.40	118.65	118.81	121.47	112.14	136.64
2	W - Tryptophan	NHα	CO	α	β	ε1	δ1	γ	δ2	ε3	ζ3	η2	ζ2	ε2
	^{1}H	7.96		4.30	3.00/3.09	10.79	6.99			7.52	6.97	7.07	7.34	
	$^{13C}/^{15N}$	117.24	171.53	55.19	27.42	131.20	123.90	110.66	127.56	118.65	118.81	121.47	112.14	136.64
3	W - Tryptophan	NHα	CO	α	β	ε1	δ1	γ	δ2	ε3	ζ3	η2	ζ2	ε2
	^{1}H	8.22		4.32	3.12/3.27	10.82	7.11			7.58	7.00	7.08	7.36	
	$^{13C}/^{15N}$	117.96	171.73	55.67	27.01	131.23	123.96	110.69	127.46	118.69	118.81	121.47	111.88	136.56
4	R - Arginine	NHα	CO	α	β	γ	δ	ε	ζ	η1	η2			
	^{1}H	8.32		3.99	1.71/1.86	1.41	3.07	7.61						
	$^{13C}/^{15N}$	116.86	171.75	54.07	27.99	25.62	40.86	85.03						
5	R - Arginine	NHα	CO	α	β	γ	δ	ε	ζ	η1	η2			
	^{1}H	8.18		4.08	1.71/1.85	1.53	3.11	7.68						
	$^{13C}/^{15N}$	116.05	171.66	53.74	28.31	25.54	40.86	84.92						
6	R - Arginine	NHα	CO	α	β	γ	δ	ε	ζ	η1	η2			
	^{1}H	8.11		3.95	1.58/1.68	1.25/1.36	3.00	7.56						
	$^{13C}/^{15N}$	116.54	171.26	54.22	28.12	25.37	40.70	84.89						

Table S9. Full assignment of c(WWWKKK) in SDS-d25 micelles.

c(WWWKKK)														
Residue #	Amino acid	Chemical shift (δ)												
1	W - Tryptophan	NHα	CO	α	β	ε1	δ1	γ	δ2	ε3	ζ3	η2	ζ2	ε2
	1H	8.12		4.27	3.17/2.81	9.84	7.12			7.41	6.95	7.00	7.34	
	13C/15N	119.05		55.24		128.72	123.39	108.80	127.60	117.91	118.89	118.92	111.65	136.07
2	W - Tryptophan	NHα	CO	α	β	ε1	δ1	γ	δ2	ε3	ζ3	η2	ζ2	ε2
	1H	7.91		4.42	2.48/2.78	9.84	7.36			7.19	6.49	6.91	7.21	
	13C/15N	116.67		54.80		128.78	111.73	111.46	127.41	117.96	123.19	121.54	111.42	135.88
3	W - Tryptophan	NHα	CO	α	β	ε1	δ1	γ	δ2	ε3	ζ3	η2	ζ2	ε2
	1H	7.91		4.71	3.18/3.44	9.84	7.28			7.34	7.00	7.06	7.37	
	13C/15N	116.67				128.72	123.90	109.75	128.2	111.65	118.92	121.49	111.75	136.00
4	K -Lysine	NHα	CO	α	β	γ	δ	ε	ζ	ε3	ζ3	η2	ζ2	ε2
	1H	7.81		3.90	1.60	1.02	1.48/1.64	2.81	7.33					
	13C/15N	120.20		56.03	29.52	22.21		39.38	160.04					
5	K -Lysine	NHα	CO	α	β	γ	δ	ε	ζ					
	1H	7.92		4.12	1.70	1.27/1.37	1.62	2.91	7.37					
	13C/15N	116.67		54.23	30.49	22.56	26.13	39.47	160.04					
6	K -Lysine	NHα	CO	α	β	γ	δ	ε	ζ					

	1H	7.22		3.92	1.10/1.20	0.51/0.70	1.04/1.22	2.45/2.58	7.23						
	13C/15N	117.70		53.59	31.49	21.56	25.88	39.30	160.00						

c(WWWKKK)															
Residue #	Amino acid	Chemical shift (δ)													
1	W - Tryptophan	NHα	CO	α	β	ε1	δ1	γ	δ2						
	^{1}H	8.12		4.27	3.17/2.81	9.84	7.12			7.41	6.95	7.00	7.34		
	^{13}C/^{15}N	119.05		55.24		128.72	123.39	108.80	127.60	117.91	118.89	118.92	111.65	136.07	
2	W - Tryptophan	NHα	CO	α	β	ε1	δ1	γ	δ2						
	^{1}H	7.91		4.42	2.48/2.78	9.84	7.36			7.19	6.49	6.91	7.21		
	^{13}C/^{15}N	116.67		54.80		128.78	111.73	111.46	127.41	117.96	123.19	121.54	111.42	135.88	
3	W - Tryptophan	NHα	CO	α	β	ε1	δ1	γ	δ2						
	^{1}H	7.91		4.71	3.18/3.44	9.84	7.28			7.34	7.00	7.06	7.37		
	^{13}C/^{15}N	116.67				128.72	123.90	109.75	128.2	111.65	118.92	121.49	111.75	136.00	
4	K -Lysine	NHα	CO	α	β	γ	δ	ε	ζ						
	^{1}H	7.81		3.90	1.60	1.02	1.48/1.64	2.81	7.33						
	^{13}C/^{15}N	120.20		56.03	29.52	22.21		39.38	160.04						
5	K -Lysine	NHα	CO	α	β	γ	δ	ε	ζ						
	^{1}H	7.92		4.12	1.70	1.27/1.37	1.62	2.91	7.37						
	^{13}C/^{15}N	116.67		54.23	30.49	22.56	26.13	39.47	160.04						
6	K -Lysine	NHα	CO	α	β	γ	δ	ε	ζ						
	^{1}H	7.22		3.92	1.10/1.20	0.51/0.70	1.04/1.22	2.45/2.58	7.23						
	^{13}C/^{15}N	117.70		53.59	31.49	21.56	25.88	39.30	160.00						

Table S10. Full assignment of c(WKWKWK) in SDS-d25 micelles.

c(WKWKWK)													
Residue #	Amino acid	Chemical shift (δ)											
1	W - Tryptophan	NHα	CO	α	β	ε1	δ1	γ	δ2	ε3	ζ3	η2	ζ2	ε2
	^{1}H			4.48	3.24/3.41	9.93	7.30			7.64	7.02	6.99	7.36	
	^{13}C/^{15}N			55.96	48.99	129.57	123.77	109.08	128.02	117.67	119.03	121.55	111.88	136.17
2	K -Lysine	NHα	CO	α	β	γ	δ	ε	ζ					
	^{1}H			3.88	1.08	0.38/0.47	1.06/1.15	2.58	7.26					
	^{13}C/^{15}N			54.55	30.22	21.28	26.08	39.28	96.16					

Table S11. Full assignment of c(WRWRWR) in SDS-d25 micelles.

c(WRWRWR)													
Residue #	Amino acid	Chemical shift (δ)											
1	W - Tryptophan	NHα	CO	α	β	ε1	δ1	γ	δ2	ε3	ζ3	η2	ζ2	ε2
	^{1}H	7.31		4.50	3.32/3.41	9.89	7.31			7.68	7.03	6.98	7.36	
	^{13}C/^{15}N					129.50	123.96	109.28	128.19	117.80	119.04	121.25	111.71	136.11
2	R - Arginine	NHα	CO	α	β	γ	δ	ε	ζ	η1	η2			
	^{1}H	7.19		3.92	1.15	0.48	2.44	6.53						
	^{13}C/^{15}N			54.37	27.92	23.30	2.56	83.97						

Table S12. Full assignment of c(WWWRRR) in SDS-d25 micelles.

c(WWWRRR)													
Residue #	Amino acid	Chemical shift (δ)											
1	W - Tryptophan	NHα	CO	α	β	ε1	δ1	γ	δ2	ε3	ζ3	η2	ζ2	ε2
	^{1}H	8.03		4.26	2.77/3.00	9.73	7.08			7.40	6.95	6.99	7.32	
	^{13}C/^{15}N	118.8			40.71	128.67	123.64	109.05		118.10	121.45	121.46	118.16	136.16
2	W - Tryptophan	NHα	CO	α	β	ε1	δ1	γ	δ2	ε3	ζ3	η2	ζ2	ε2
	^{1}H	7.40		4.44	2.62/2.74	9.70	7.18			7.30				
	^{13}C/^{15}N	127.06				128.90	123.88							136.04
3	W - Tryptophan	NHα	CO	α	β	ε1	δ1	γ	δ2	ε3	ζ3	η2	ζ2	ε2
	^{1}H	7.17		4.66	3.24	9.67	7.17			7.40	6.95	6.99	7.32	
	^{13}C/^{15}N					128.79	123.84	109.50		118.10	121.45	121.46	118.16	135.96
4	R - Arginine	NHα	CO	α	β	γ	δ	ε	ζ	η1	η2			
	^{1}H	7.71		3.91	1.66/1.53	1.13/1.20	2.90	6.87						
	^{13}C/^{15}N	120.81			27.52	24.45	40.62	84.19						
5	R - Arginine	NHα	CO	α	β	γ	δ	ε	ζ	η1	η2			
	^{1}H	7.93		4.10	1.72/1.84	1.51	3.14	7.07						
	^{13}C/^{15}N	116.93				25.07	40.70	83.91						
6	R - Arginine	NHα	CO	α	β	γ	δ	ε	ζ	η1	η2			
	^{1}H	7.29		3.94	1.15	0.78/0.95	2.61/2	6.64						
	^{13}C/^{15}N	117.44			24.32	23.95	40.28	84.02						

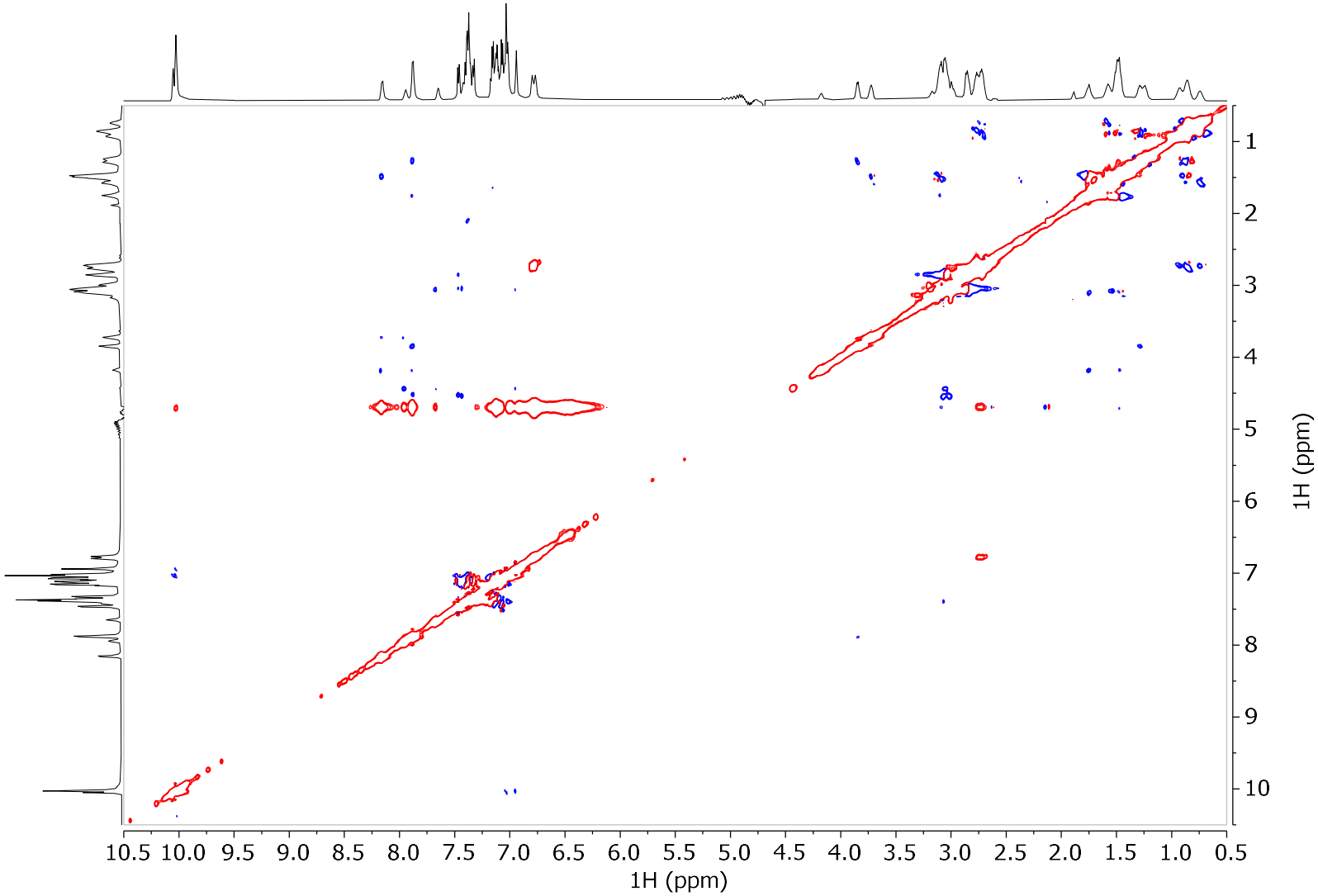

Figure S2. ROESY spectrum of c(WWWRRR) in water at 75 ms mixing time.

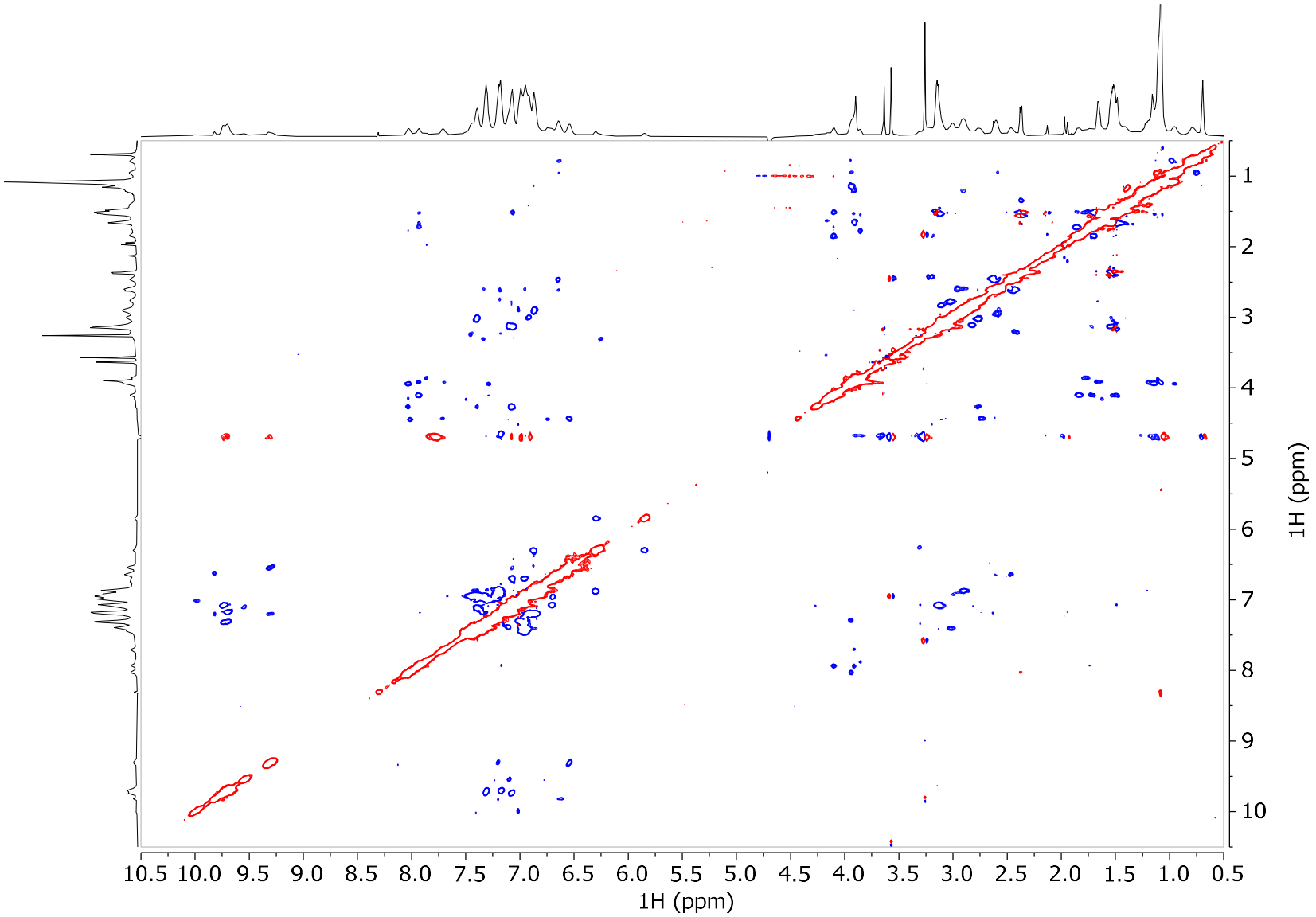

Figure S3. ROESY spectrum of c(WWWRRR) in SDS-d25 at 75 ms mixing time.

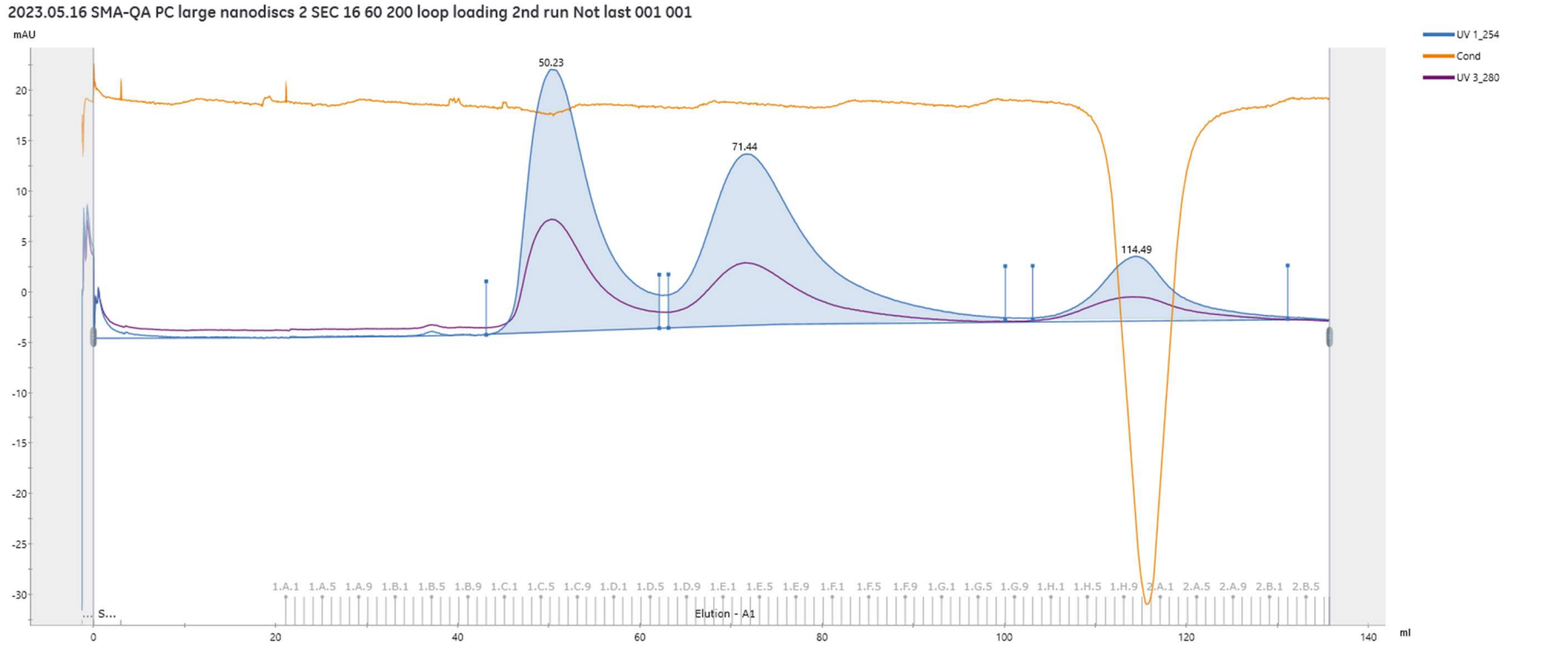

Peak Table - UV 1_254

Peak	Retention ml	Area ml*mAU	Area %	Ext coeff. mg ml⁻¹ cm⁻¹	Fraction(s)	Volume ml	Conductivity mS/cm
Peak A	50.225	210.7	42.67		1.B.11 - 1.D.5	19.002	11.45
Peak B	71.438	224.3	45.42		1.D.7 - 1.G.7	37.001	11.46
Peak C	114.488	58.83	11.91		1.G.11 - 2.B.2	28.000	11.19

Figure S 4. SEC chromatography output for SMA-QA DMPC nanodiscs at approximately 30 nm diameter.

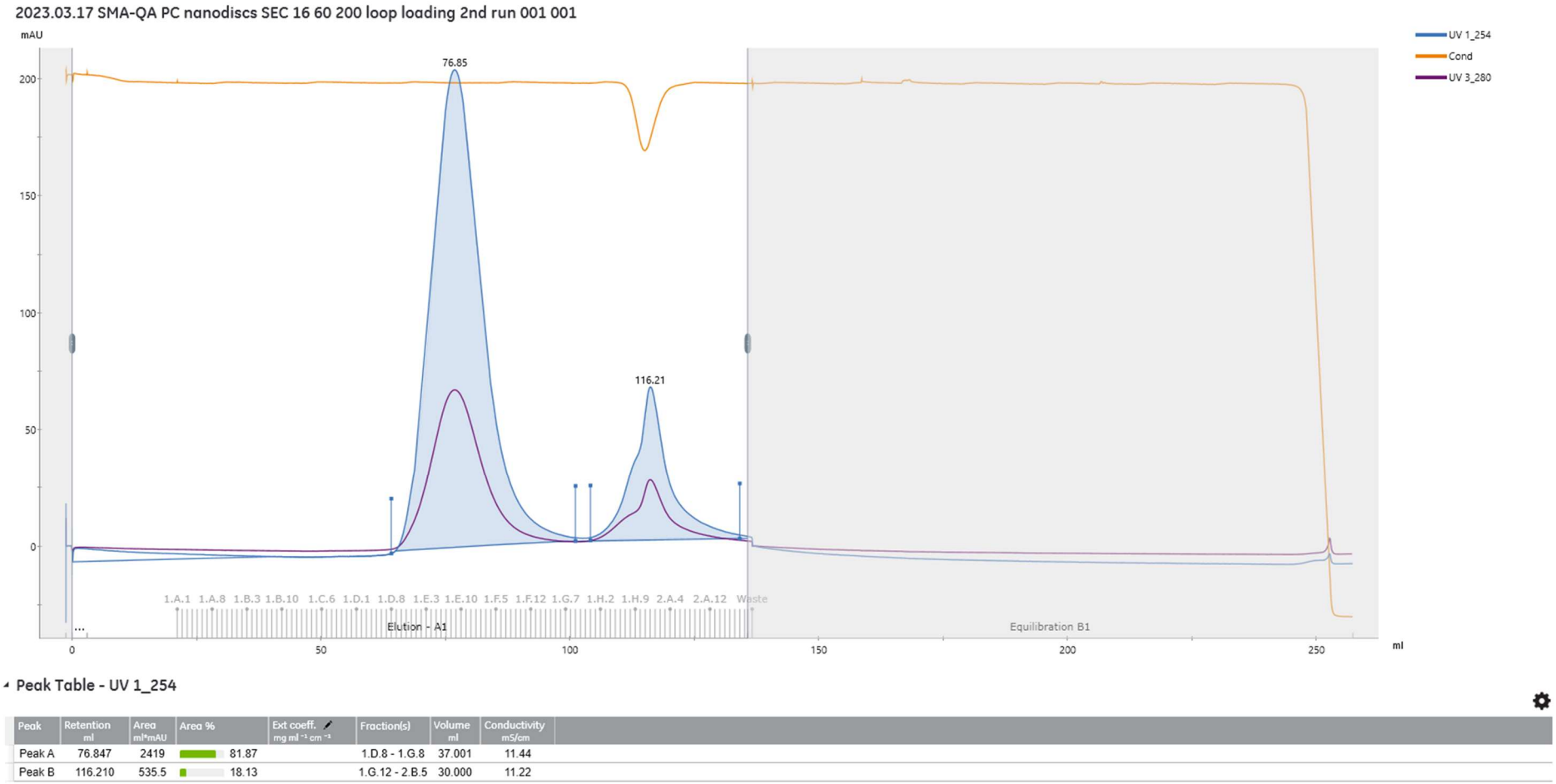

Peak Table - UV 1_254

Peak	Retention ml	Area ml*mAU	Area %	Ext coeff. mg ml⁻¹ cm⁻¹	Fraction(s)	Volume ml	Conductivity mS/cm
Peak A	76.847	2419	81.87		1.D.8 - 1.G.8	37.001	11.44
Peak B	116.210	535.5	18.13		1.G.12 - 2.B.5	30.000	11.22

Figure S 5. SEC chromatography output for SMA-QA DMPC nanodiscs at approximately 10 nm diameter.

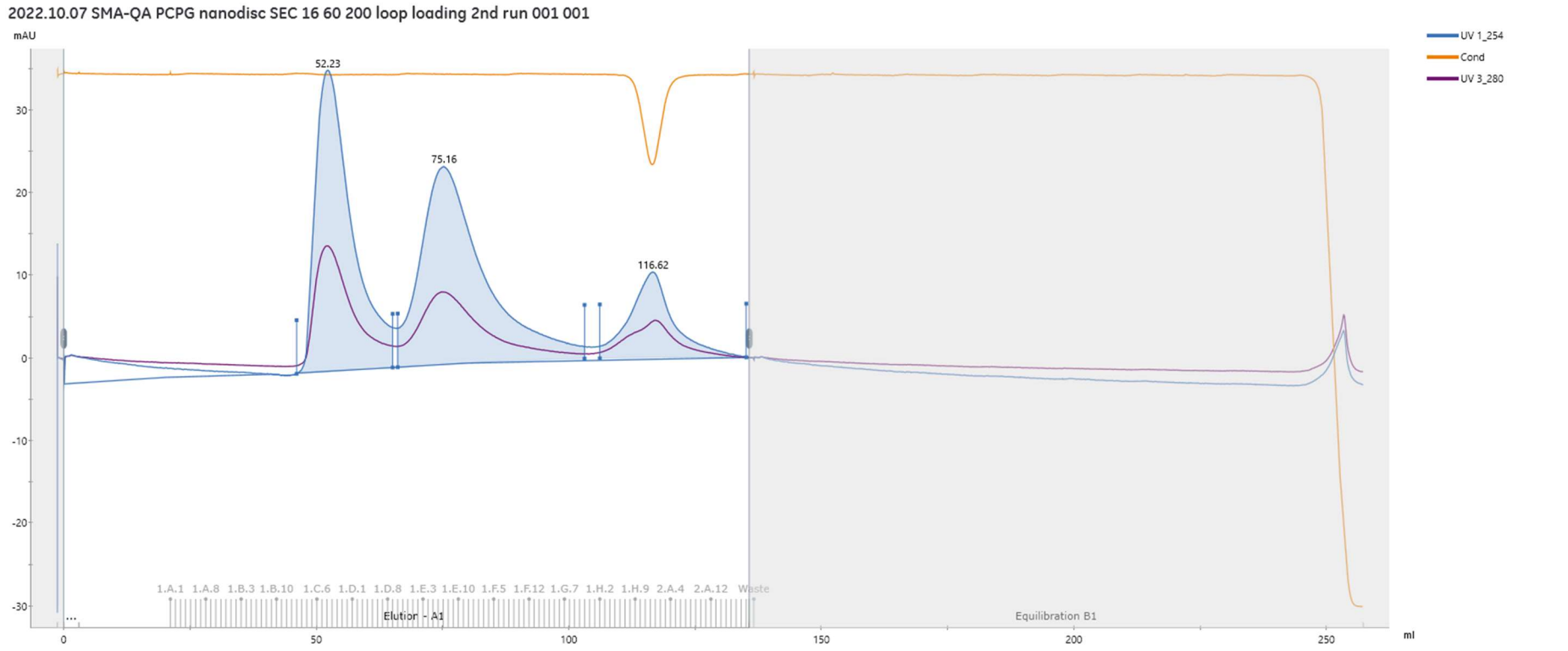

Peak Table - UV 1_254

Peak	Retention ml	Area mAU*ml	Area %	Ext coeff. mg ml⁻¹ cm⁻¹	Fraction(s)	Volume ml	Conductivity mS/cm
Peak A	52.234	305.6	40.24		1.C.2 - 1.D.8	19.001	11.62
Peak B	75.162	350.7	46.19		1.D.10 - 1.G.10	36.997	11.63
Peak C	116.617	103.1	13.57		1.H.2 - 2.B.6	29.004	11.33

Figure S 6. SEC chromatography output for SMA-QA DMPC/5% DMPG nanodiscs at approximately 10 nm diameter.

Figure S 7. 3-state phi/psi distribution prediction of the secondary structure as alpha helix, beta sheet and positive phi type of conformations in TALOS+(N). This model suggests significant changes for the lysine containing peptides in SDS compared to water, with DMSO in between, which was not the case for the direct secondary structure prediction in Figure 2.

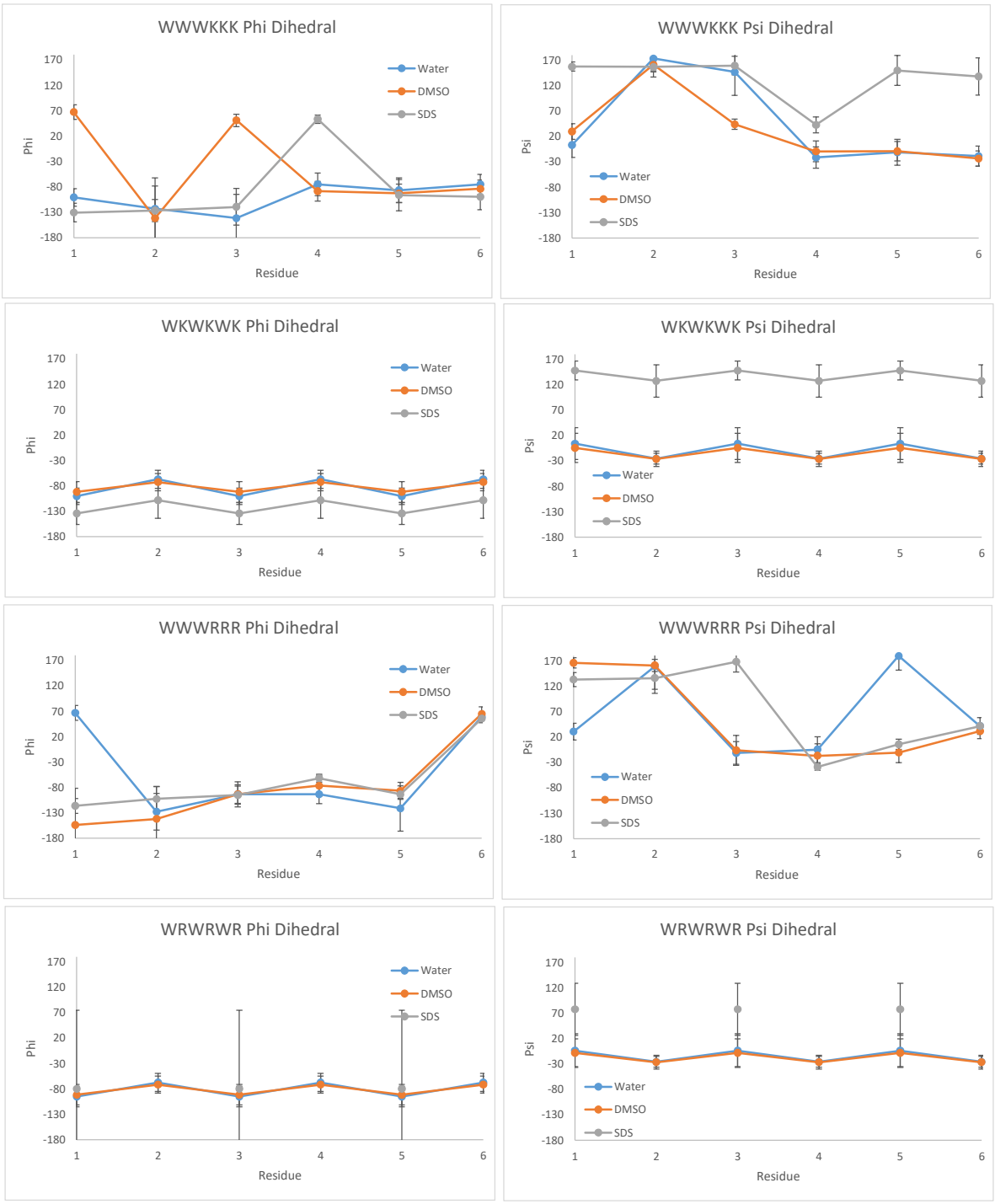

Figure S 8. Protein Backbone Torsion Angle Prediction in TALOS+(N), suggesting phi- and psi dihedral angles.

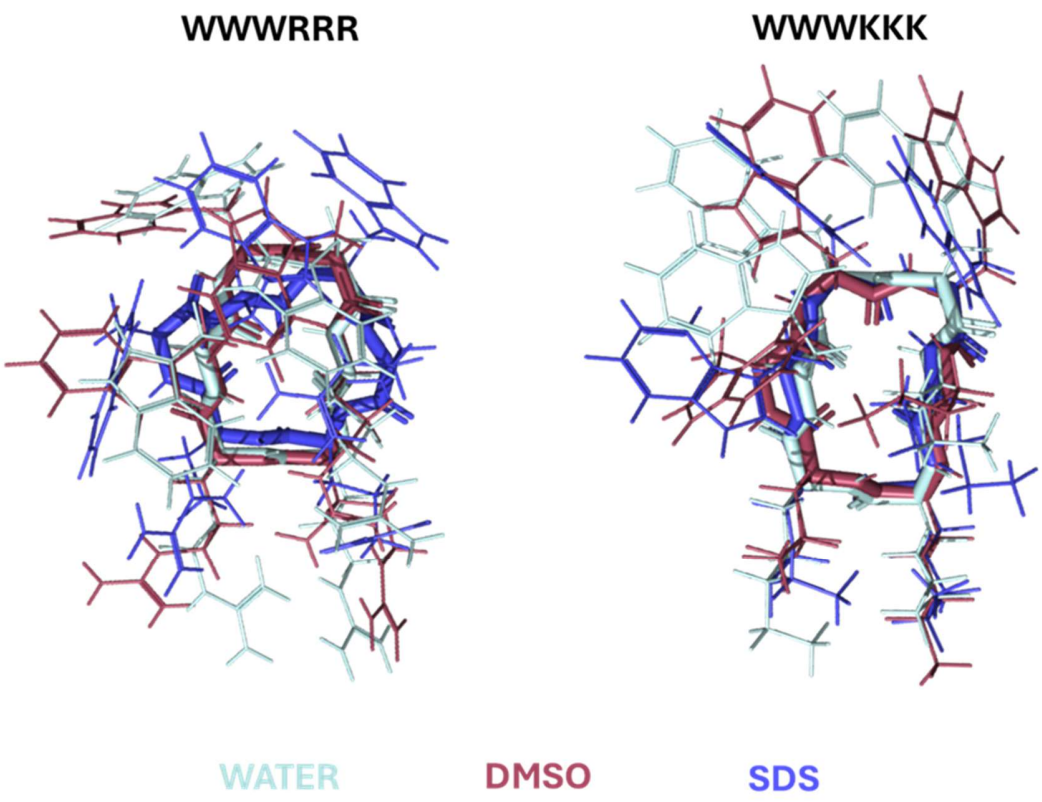

Figure S 9. Superimposed representations of average from the ten lowest energy conformations based on NOE constraints of c(WWWKKK) and c(WWWRRR) in water, DMSO, and SDS micelles.